

Time-Dependent Behaviour of Brittle Rocks Based on Static Load Laboratory Tests

Chrysothemis Paraskevopoulou  · Matthew Perras · Mark Diederichs · Simon Loew · Tom Lam · Mark Jensen

Received: 29 June 2016 / Accepted: 10 August 2017 / Published online: 22 August 2017
© Springer International Publishing AG 2017

Abstract Cumulative elastic and inelastic strain and associated internal stress changes as well as damage evolution over time in brittle rocks control the long-term evolution of the rockmass around underground openings or the land surface settlement. This long-term behaviour is associated with time-dependent deformation and is commonly investigated under static load (creep) conditions in laboratory scale. In this study, low Jurassic and Cobourg limestone samples were tested at different static load levels in unconfined conditions to examine the time to failure. Comparisons are made with longterm testing data in granites and limestones associated with the Canadian nuclear waste program and other data from the literature. Failure typically occurred within the time

limits of the test program (4 months) with axial (differential) stress levels near or above the crack damage threshold (CD) estimated from baseline testing. The results also suggest that the time to failure of limestone is longer than that of granite at a given driving stress. Further insight into samples that did not reach failure was investigated and it was found that there was a clear division between failure and no failure samples based on the Maxwell viscosity of the samples tested (indicating that viscosity changes near the yield threshold of these rocks. Furthermore, samples showed a clear tendency towards failure within minutes to hours when loaded above CD and no failure was shown for samples loaded below CI (crack initiation threshold). Samples loaded between CD and CI show a region of uncertainty, with some failing and other not at similar driving stress-ratios. Although such testing is demanding in terms of setup, control of conditions, continuous utilization of test and data acquisition equipment and data processing, it yields important information about the long-term behaviour of brittle rocks, such as the expect time to failure and the visco-elastic behaviour. The information presented in this paper can be utilized for preliminary numerical studies to gain an understanding of potential impact of long-term deformations.

C. Paraskevopoulou (✉)
School of Earth and Environment, University of Leeds,
Leeds, UK
e-mail: C.Paraskevopoulou@leeds.ac.uk;
chrys.parask@gmail.com

M. Perras · S. Loew
Institute of Geology, Swiss Federal Institute of
Technology, Zurich, Switzerland

M. Diederichs
Department of Geological Sciences and Geological
Engineering, Queen's University, Kingston, ON, Canada

T. Lam · M. Jensen
Nuclear Waste Management Organization, Toronto, ON,
Canada

Keywords Long-term behaviour · Time-dependency · Static load testing · Laboratory testing · Creep · Visco-elastic parameters

1 Introduction

The deformation and strength of rock and rockmasses are considered to be time-dependent (Hoek and Brown 1980; Ladanyi and Gill 1988; Lajtai et al. 1991; Boukharov et al. 1995; Pellet et al. 2005; Anagnostou 2007; Barla et al. 2010; Paraskevopoulou 2016). In practice, however, the effect of time is usually assumed to be negligible for brittle rocks; thus engineers and scientists usually tend to neglect it during the design process of a project (Lajtai et al. 1991). During the last half century while the design and construction of deep underground openings has increased; the interest in the long-term behaviour and strength of the surrounding rockmass has also increased. In cases where the desired lifetime of a project significantly exceeds 100 years, as is the case with nuclear waste repositories, considering the evolution and performance of long-term strength of the host rock is of crucial significance. A better understanding of the long-term rock deformability in the design and construction of nuclear waste repositories is a key behavioural aspect for predicting the ability of the rock to isolate the waste from the biosphere (Damjanac and Fairhurst 2010).

Especially in cases where the in situ stress is relatively high with respect to the short-term strength of the host rock (Lajtai and Schmidtke 1986) this situation could conceivably lead to time dependent deformation, degradation and post-construction failures that can lead to cost overruns (Paraskevopoulou and Benardos 2013). Creating methods and engineering tools to be used for the prediction of the long-term performance behaviour of the rockmass such as those that other researchers (Schmidtke and Lajtai 1985; Lajtai 1990; Dusseault and Fordham 1993; Heap et al. 2011) have already highlighted would be significant advance in underground excavation design.

The purpose of this paper is to investigate the long-term performance behaviour of low porosity brittle rocks with emphasis on the procedures and methods to estimate and predict the long-term strength of rocks. This was done by performing a series of static load creep tests, at varying differential stress states, giving more insight into the time-dependent behaviour of brittle rock. In the literature, the majority of the data for static load creep tests have been performed at room temperature in uniaxial conditions with zero confinement. In this study we follow this approach. The long-

term strength in unconfined conditions is investigated, while controlling and recording the impact of the environmental conditions (i.e. temperature and humidity), and the visco-elastic parameters for the Burgers model are derived. For samples closer to the short-term yield stress, failure is ultimately observed and time-to-failure noted. This study focuses on two different limestones; the Jurassic limestone from Switzerland and the Cobourg limestone from Canada. The selection of the rock types was based on the possibility that the Cobourg limestone could serve as a host rock for a proposed Low and Intermediate Nuclear Waste Repository in Canada and is also representative of rock units that may be candidates for high level storage. The Jurassic limestone was also used to examine the testing procedure and to serve as comparative limestone and also compliment the data from the Cobourg samples.

2 Background

2.1 Time-Dependency in Rock Mechanics

In the literature (Singh 1975; Aydan et al. 1993; Einstein 1996; Malan et al. 1997; Hudson and Harrison 1997; Hagros et al. 2008; Brantut et al. 2013; Paraskevopoulou 2016) time-dependency of rock under load has been widely discussed. Since the late 1930s, researchers started investigating the effect of time in rock behaviour, trying to apply the theory of creep widely studied and reported on metals (Weaver 1936) to rock behaviour. It was not until 1939 when Griggs undertook laboratory experiments to examine the phenomenon of creep of rocks. He constructed two apparatus and performed tests on limestone, anhydride, shale and chalk. He also examined recrystallization under creep conditions at high pressure.

At the excavation scale, addressing the effect of time in tunnelling and mining engineering has been studied since the 1950s where researchers introduced the idea of ‘stand-up time’ in tunnel stability. In 1958, Lauffer suggested the time and span was one of the most important parameter in tunnel stability. The ‘stand up time’, a reflection of time-dependent weakening, was also included in the rockmass classification systems (Bieniawski 1974; Barton 1974; Palmstrom 1995), giving emphasis on time and its effects by producing charts illustrating the time frame of stable unsupported spans.

Since the 1960s many researchers (Widd 1966; Bieniawski 1967; Wawesik 1972; Singh 1975; Peng 1973; Kranz and Scholz 1977; Schmidtke and Lajtai 1985; Lau and Conlon 1997; Lau et al. 2000; Berest et al. 2005; Cristescu 2009) have investigated the influence of time on the long-term strength of rock by performing laboratory testing on rock samples, typically using static load (creep) tests by sustaining a constant stress condition. In accordance with this practice, new constitutive and numerical time-dependent models were introduced based on the experimental results and data (Ottosen 1986; Boukharov et al. 1995; Pellet et al. 2005; Debenarndi 2008; Sterpi and Gioda 2009). These models attempt to capture and reproduce the behaviour of laboratory tests on the rocks including time.

2.2 Defining and Explaining Time-Dependency in Rocks

In practice, there is often a miscomprehension and misinterpretation of the different time-dependent phenomena and the mechanisms acting and resulting in weakening rock and the rockmass over time. This section serves as an attempt to redefine and give more insight into the various time-dependent phenomena, their mechanisms, responses and key characteristics. Figure 1 presents a composite nomenclature that describes the various mechanisms that can possibly appear to be time-dependent under the appropriate conditions. The parameters that can define the type of time-dependency can be generalized to state-change and property-change. The time-dependent processes can result, for example, in a changing stress-state (i.e. stress relaxation) or a change in the intrinsic properties of the rock material (i.e. decrease in cohesion). These changes can be further categorized according to their reversibility or recoverability using such terms as elastic, inelastic and irreversible and may give rise to visco-elastic or visco-plastic strains. The physical response can be represented as creep (shear strain), contraction or dilation (volumetric strains) over time as well as relaxation (reduction in shear stress under sustained strain) and degradation (strength loss of softening) depending on loading and boundary conditions.

The micro-mechanical mechanisms, however, that can lead to these responses tend to vary according to the boundary conditions. For instance, the solid

rheology (e.g. lattice distortion, dislocation slip, van der Vaal's bonds and/or solid diffusion) may be damaged by new cracks that initiate or pre-existing ones propagate while pores, grain boundaries and pre-existing cracks creating discontinuum elements. In addition, the physicochemical changes although can be temporal, rheological and chemical alterations in the micro-scale can lead to swelling, weakening, strain-softening and hardening. The rate and the magnitude of the time-dependent performance of rock materials are controlled by other environmental, physical and loading conditions (e.g. chemistry, fluid mobility, stress deviator, temperature, pressure, humidity and confinement).

As noted and as implied in Fig. 1 that time-dependent phenomena can be a combination of many factors that can result in various physical responses. For instance, in a tunnelling environment, after excavation and installation of the temporary support, there may be observed an increasing deformation in the tunnel walls with time and at a distance farther from the face than static analysis would predict. This continuous deformation may be the result of creep (time-dependent shear strain) or may also be the result of volume increase (i.e. time-dependent dilation), physicochemical reactions (i.e. swelling) or even due to the evolution of macro-cracks in the surrounding rockmass (degradation) allowing the stress to relax or ultimately yield. More than one time-dependent phenomena can potentially act at the same time and thus the time-dependent deformation is the cumulative result of these active phenomena. Differentiating and recognizing these phenomena can be a complex process but the suite of issues presented in Fig. 1 should be taken into consideration when investigating possible deformation or failure modes.

The overall physical response can be a combination/integration of the mechanisms that influence the long-term behaviour of intact rock and rockmasses and include:

- creep during which visco-elastic behaviour governs where time-dependent, inelastic strains and 'indefinite' deformation take place and/or visco-plastic yield where time-dependent plastic strains occur that lead to permanent deformation (Pellet et al. 2005).
- dilation or contraction where volume change takes place over time usually caused by the change of

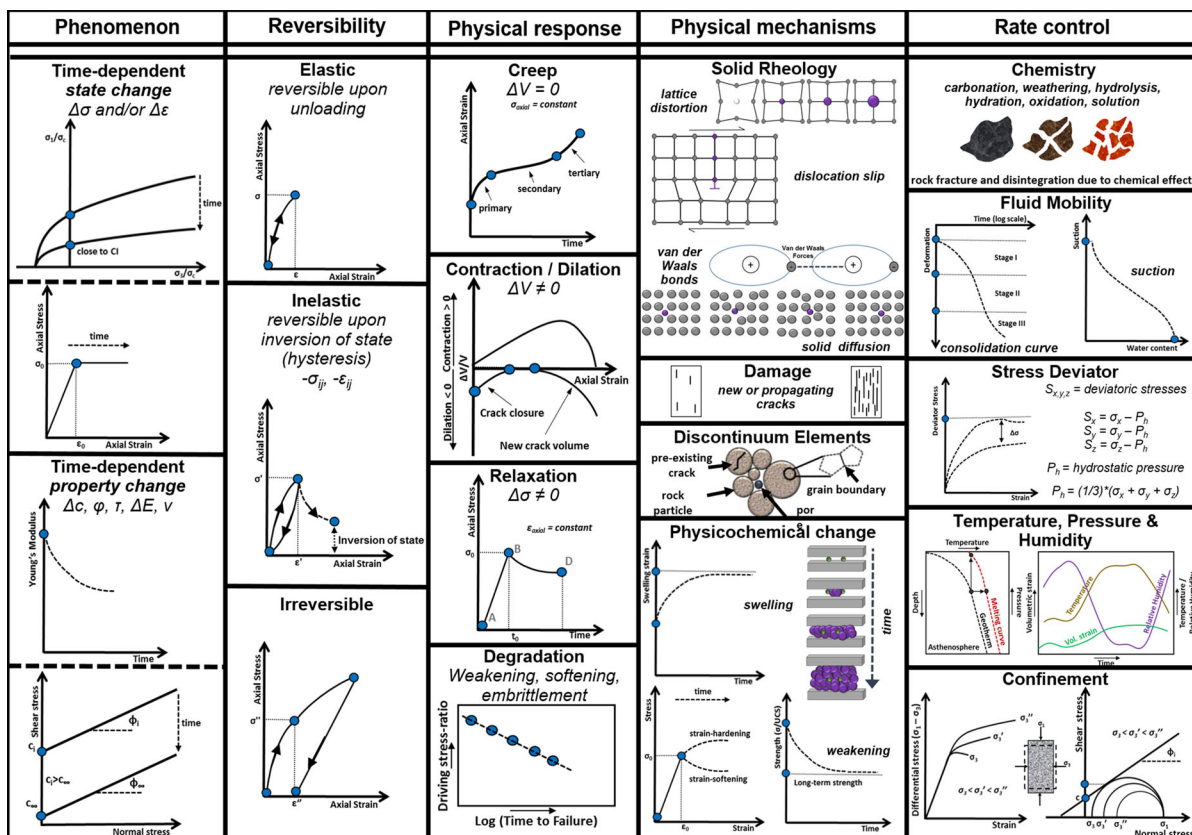


Fig. 1 Nomenclature, Defining time-dependent phenomena and the conditions and mechanisms that affect and govern the rock behaviour

- stress resulting in the propagation and interaction of cracks (dilatation) or the closure of the existence ones (contraction) (Van and Szarka 2006); and;
- relaxation where the reduction of the stress with time under sustained strain is controlled by the internal creep processes aimed at relieving the stored commonly elastic energy (Lin 2006).
 - mechanical property degradation where strength and/or stiffness change as a result of damage processes that accompany or occur as a result of the above phenomenon (Damjanac and Fairhurst 2010).

This paper focuses on investigating the time-dependent behaviour of brittle rocks under a constant (controlled) stress-state by performing a series of uniaxial static load (creep) tests on two types of limestone. The main focus is on the creep behaviour and associated degradation and how these related mechanisms influence the time to failure of the laboratory samples.

2.3 Creep of Rocks

Creep was initially observed in metals (da Andrade 1910). In geological sciences creep is usually related to long-term loading which is evident in nature in landslides, volcanoes, rockmassifs etc. (Amitrano and Helmstetter 2006). Creep can be defined as the time-dependent distortion of a material that is subjected to constant deviatoric stress that is less than its short-term strength and is related to the irreversible deformation under constant stress over time ('flow'). During creep, visco-elastic behaviour governs where time-dependent, reversible, elastic strains take place (primary stage in Fig. 2). Elasto-viscous behaviour (secondary stage) results in partially recoverable (upon load reversal for example) and potentially indefinite deformation. Visco-plastic yield (tertiary stage) results in time-dependent plastic strains leading to failure and sometimes permanent deformation when one focuses to incremental or small time periods (Pellet et al.

2005). Strength degradation during the first stages of creep can ultimately lead to brittle failure in time.

Creep strain can seldom be fully recovered (Glamheden and Hokmark 2010) when the visco-elastic regime is extensive enough where irrecoverable strains are allowed to be developed. According to Amitrano and Helmstetter (2006) rock materials exhibiting creep deform with different strain rates at different stages during the test. The general shape of the creep curve however, is typical for most materials as illustrated in Fig. 2 and there are only a few differences in the general form for all rock types. However, the strain magnitude and the duration of each of the creep stages (primary, secondary, and tertiary) can independently be observed depending on the nature of the rock.

The creep stages begin after the load has been applied and kept constant and typically this is dominated by elastic strains. When the applied load becomes constant, the strains increase with a decreasing rate; this period is called primary (transient) creep. When primary creep approaches a constant strain rate (almost a steady rate) the transition to the secondary creep (or steady rate) takes place. The material can yield in an accelerating or even brittle manner as the strain rate starts to accelerate. This latter stage is often referred to as tertiary creep although the processes involved may not be related to creep mechanics. These stages are characteristics of and vary for each rock type (Sofianos and Nomikos 2008). It should be noted in some rock materials, usually brittle, the secondary creep is not clear and always observed and failure occurs due to the accumulation of irreversible (plastic) strains over time. For other rocks the tertiary creep stage is never reached or it could be reached after a very long period of time (i.e. ductile materials as rock

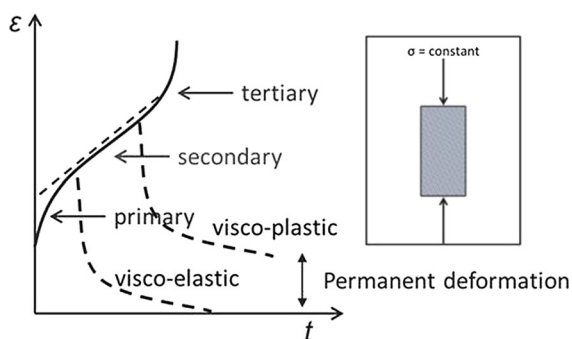


Fig. 2 The three stages of creep (primary, secondary, tertiary) of a material subjected under constant load

salt). As Lockner (1993) reported it can be a transition from primary to tertiary creep with no second state or the deformation can be purely characterized by a steady strain rate as in the secondary stage.

2.3.1 Time-Dependent Formulations and Models

Empirical models and relations are commonly used to describe creep behaviour and are usually based on experimental and laboratory data from static load (creep tests). Such models are generally specific for a given rock type. These models' utility is to describe the time-dependent performance of these rocks under various stresses producing a general trend over time between stress and strains (Amitrano et al. 1999). The formulations of these models and laws available in the literature can be categorized into three main groups: (a) empirical functions (Aydan et al. 1996; Singh et al. 1998), based on curve fitting of experimental data, usually static load (creep) tests, (b) rheological models (Ottosen 1986; Gioda 1981; Chugh et al. 1987), consisting of mechanical analogues such as elastic springs, viscous dashpots, plastic sliders and brittle yield elements coupled in series or in parallel and (c) general theories (Perzyna 1966) and models based on general theories (Debernardi 2008) that are considered to be the most advanced aspects of numerical modelling that are not limited to specific cases and can be implemented in various numerical analysis codes (i.e. Finite Element and Finite Difference codes). Empirical models are most commonly used, although these models are derived from test data for certain rock types and can be used as a first preliminary design tool but are of limited application for other rock types and certainly for other factors not considered in the laboratory test.

2.3.1.1 Burgers Rheological Model for Creep Behaviour Time-dependency was initially studied in terms of rheology, the science of deformation and flow of matter assuming that deformations are caused due to the intrinsic viscous nature of materials (Goodman 1980). The term is derived from the Greek word 'rheos' which means flow. Viscosity is a measure of a matter's resistance to flow, it describes the internal friction of the moving matter and controls the deformation rate. The rheological behaviour of ideal rock materials approximates the visco-elastic stress/strain response. However, in reality this is

seldom the case as typical rock material behaviour is characterized by inelasticity or non-linear deformation due to the presence of microcracks, voids or flaws.

The idealized creep behaviour (under uniaxial compression) is often represented mathematically by the Burgers model. This model is a combination of the Kelvin (delayed manifestation of a constant static response to altered boundary conditions) and Maxwell (continued strain rate or relaxation over time under static boundary conditions) models in series (as illustrated in Fig. 3). According to Goodman (1980) the strain occurring during constant loading condition through time can be expressed using Eq. 1, where: ε_1 is the axial strain, σ_1 is the constant axial stress, K is the bulk modulus associated with the volumetric deformation under hydrostatic conditions, η_K is Kelvin's model viscosity, η_M is Maxwell's model viscosity, G_K is Kelvin's shear modulus, G_M is Maxwell's shear modulus. η_K , η_M , G_K , G_M are the visco-elastic parameters and are considered properties of the rock.

$$\varepsilon_1(t) = \frac{2\sigma_1}{9K} + \frac{\sigma_1}{3G_M} + \frac{\sigma_1}{3G_K} - \frac{\sigma_1}{3G_K} e^{-\left(\frac{G_K}{\eta_K}t\right)} \quad (1)$$

Following Goodman's approach, the visco-elastic parameters for the Burgers model (η_K , η_M , G_K , G_M) can be derived by fitting the experimental results of static load (creep) tests to the curve of Eq. 1 (shown in Fig. 3) at different time increments and the corresponding strain intercepts.

The three afore-described stages of creep follow the instantaneous response (0th stage) due to the changed boundary conditions during loading leading to the constant load. These stages can be interpreted from the idealized creep behaviour described above and simulated as follows:

- 1st stage or primary or transient creep where the delayed adjustment to a new equilibrium state takes place through visco-elastic (reversible) deformation, and may be accompanied by some irreversible behaviour, resulting in strain accumulation with decreasing rate over time. This stage is commonly simulated with the Kelvin model analogue.
- 2nd stage or secondary creep where the material exhibits a consistent strain accumulation rate over time accompanied by inelastic distortion. The duration or even existence of this stage can vary depending on the rock type transitioning from

ductile to more brittle materials. The Maxwell visco-elastic model is commonly used to phenomenologically represent this stage.

- 3rd stage or tertiary or accelerating creep where abrupt increase of strains occur (typically driving the material to rupture) due to strain-driven weakening, chemically related strength degradation and/or interaction of growing cracks. Viscoplastic models (Dragon and Mroz 1979) and/or so-called stress corrosion models (Damjanac and Fairhurst 2010) are used to simulate tertiary creep.

A Burgers model, combination of the two, can be used to reproduce stages 1 and 2 but fails to simulate stage 3 (delayed failure). Overall, rheological models are typically used to describe time-dependent creep deformation. These models provide a mathematical framework; however, they do not take into account physical mechanisms related to microcrack initiation and propagation (Paraskevopoulou et al. 2015; Paraskevopoulou et al. 2016).

2.4 Damage Evolution and Brittle Failure

The static load tests were conducted at different stress levels which were representative of driving stress to strength ratios based on a series of baseline Unconfined Compressive Strength (UCS) testing based on the ISRM (1979) suggested method.

In ductile rock materials, the deformation process is primarily related to continuum creep mechanics involving dislocation slip or migration of interstitial atoms and atomic vacancies within crystals, or weak bond migration in clay minerals (Davis et al. 2012) resulting in distortion (pure or simple shear strain) over time. In brittle rocks, however, it is generally accepted that a progressive damage, which is initially dominated by the initiation and propagation of microcracks in the direction of the maximum load, governs the deformation process leading to sudden rupture (Fairhurst and Cook 1966; Diederichs 1999; Ghazvnian 2015).

At least four distinct stages of the brittle failure process in compression tests can be identified if the stress–strain response is monitored during loading, as shown in Fig. 4. These stages are: (1) closure of pre-existing cracks; (2) linear elastic behaviour (reversible strains); (3) stable crack growth; and (4) unstable crack growth, which leads to failure and the peak strength (the

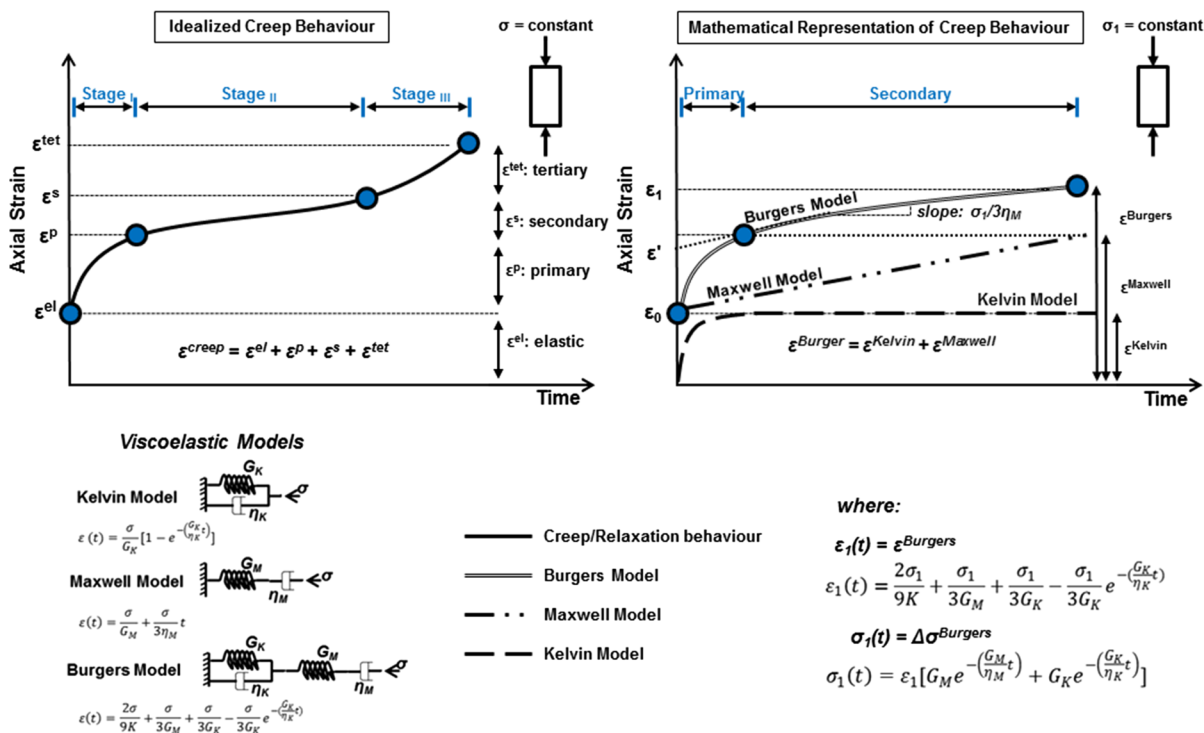


Fig. 3 Idealized creep behavioural curve (left column) and the equivalent viscoelastic components (Kelvin and Maxwell) which are combined in parallel resulting in the Burgers model

point of maximum stress). These damage or crack growth thresholds have been defined by the International Rock Mechanics Committee on Spall Prediction as CI for Crack Initiation and CD for Crack Damage respectively (Diederichs and Martin 2010). CD is, sensitive to pre-existing crack damage, sample geometry, and stress path (Diederichs 2003) whereas CI is relatively insensitive to moderate preexisting damage and other influences and is found to be 30–50% of the standard UCS, as measured in the laboratory (Brace et al. 1966; Martin 1993, 1997) for brittle rocks or by in situ back analysis (Martin et al. 1999) and CD is found to be 70–90% of the UCS (Perras and Diederichs 2014).

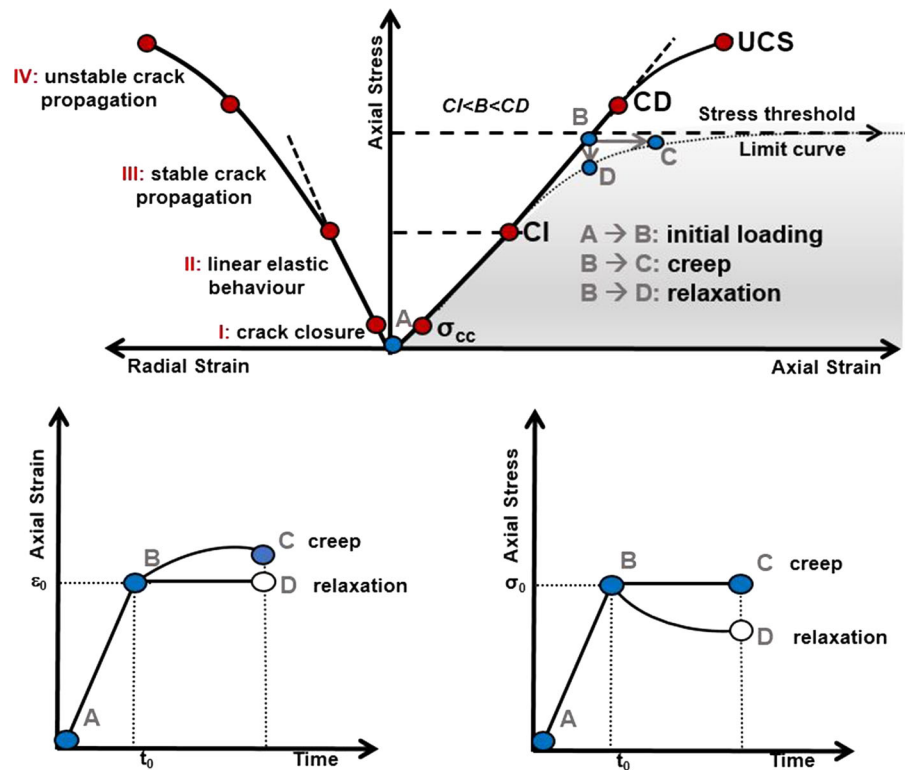
Stress–strain curves for brittle rocks can be used to determine the: (1) crack initiation stress (CI); (2) critical damage stress or axial yield stress (CD); and, (3) uniaxial compressive strength (UCS). Many researchers (Bieniawski 1967; Martin and Chandler 1994; Martin 1993; Lajtai 1998; Eberhardt et al. 1998; Diederichs 1999, 2003; Diederichs et al. 2004; Nicksiar and Martin 2012; Ghazvnian 2015) investigated the identification of the thresholds using various methods (i.e. strain-

representation of the idealized curves (right column). At the bottom the viscoelastic models are illustrated and represented mathematically

based or acoustic emission). For instance, the Crack Initiation (CI) threshold can be determined as the axial stress at reversal point of the calculated crack volumetric strain according to Martin’s (1993) and Diederichs and Martin’s (2010) approach. The deviation from linearity of the radial strain is another approach used to determine CI (Bieniawski 1967; Lajtai 1974; Diederichs et al. 2004), which is free from errors introduced by involving calculated parameters in the estimation. Critical Damage (CD), the crack coalescence and interaction threshold (Lockner et al. 1992), is determined as the axial stress at the measured volumetric strain reversal point (Bieniawski 1967; Lajtai 1974; Martin 1997).

At increasing stress levels between CI and CD the cracks accumulate and grow in a stationary rate (stable manner). However, if the load or axial stress is held constant between these thresholds, time-dependent crack growth occurs leading to time dependent deformation, as illustrated in Fig. 4. Loading above the critical damage threshold (CD) marks the growth of cracks in an unstable manner during UCS testing. If the axial stress is maintained at a stress level in excess of CD, accelerated creep rates may occur that

Fig. 4 Stress–strain response and stages of brittle rock fracture process and time-dependent behaviour of the material exhibiting: creep and/or relaxation depending on the initial loading and stress conditions, (where: σ_{cc} stress level at crack closure, CI crack initiation, CD critical damage, UCS unconfined compressive strength, σ_c applied constant stress)



can lead to a sudden failure of the specimen (Schmidtke and Lajtai 1985).

As discussed, many researchers (e.g. Brace et al. 1966; Podnieks et al. 1968; Bieniawski 1967; Martin 1997, Diederichs 2003, etc.) investigating the inelastic behaviour of rocks indicated that crack initiation and propagation plays a dominant role in understanding processes related to time-dependent behaviour.

2.4.1 Creep in Brittle Rocks

Creep strains are usually associated with the deformation sequence of the time-dependent processes, as described: the instantaneous elasticity, the primary/transient creep, the secondary/steady-state creep and the tertiary/accelerating creep (Gruden 1971), which can be the case for metals and some weak rocks (Stagg and Zienkiewicz 1986). On the contrary, the long-term behaviour of a poly-crystalline rock depends on the physical processes acting on the individual grains and the rock as a whole and the interaction of the rock grains and other structural features with their neighbours (Boukharov et al. 1995). In the case of intact (brittle) rocks, the steady-state creep or

secondary creep phase may not be visible depending on the stress level. At very high stresses, the rock may exhibit only primary creep with a sudden transfer to the tertiary stage that will result to abrupt failure.

Another aspect of the time-dependent behaviour in brittle rocks is the condition of joints and other structural weaknesses which can influence the long-term behaviour. Lajtai et al. (1991) reported that the existence of discontinuities mainly influences the instantaneous and short-term stability whereas degradation of the intact rock influences the long-term behaviour.

The degradation of the mechanical properties over time for various brittle rocks has been discussed in the literature (e.g. Bieniawski 1967; Schmidtke and Lajtai 1985; Kranz and Scholz 1977; Lau et al. 2000). Lajtai et al. (1991) observed, after performing tests on Lac du Bonnet Granite samples, that the loss of strength on a sample which is subjected under constant load for a longer period of time is not caused by the decrease of frictional resistance but that it should be attributed to the time-weakening of the intact rock.

According to Anderson (1977) the time-dependent weakening of brittle rockmasses and intact rocks is

ascribed to stress-corrosion cracking. Stress corrosion cracking is the chemically controlled crack growth in the presence of mechanical stress over time, which Charles (1959) also showed by performing experiments on glass. Lajtai and Schmidtke (1986) have shown that stresses of about 50% or more of the short-term strength of brittle rocks can trigger time-dependent stress corrosion cracking.

Another mechanism, in heterogenous rocks (polycrystalline like granite or multi-component like argillaceous limestone) is the interference of different mineral grains undergoing creep strain at different rates and through different mechanism. The internal interference between deforming grains can lead to internal damage and weakening over time and at a rate related to the creep strain rate.

2.5 Methods Used to Estimate Long-Term Strength

Goodman (1980) argued that the complete stress strain curve can also be used to predict rock failure due to creep. The existence of a ‘static fatigue limit’, has been suggested (Lajtai and Schmidtke 1986; Lajtai et al. 1991; Lau et al. 2000; Damjanac and Fairhurst 2010, etc.) as the lower bound of stress that leads to failure given the appropriate time. Below this limit (stress level) no failure occurs at any time. This is known as the long-term strength (LTS) shown in Fig. 5.

Many researchers (Potyondy 2007; Hao et al. 2014; Cristescu 2009; Paraskevopoulou et al. 2015) have estimated the lifetime (time-to-failure) of intact rocks by adopting the time-to-failure approach similar to Lajtai and Schmidtke (1986). It distributes the strength decay under long-term constant loading and results in

the creation of the static fatigue curve which relates to the specific data set and testing conditions. From a series of static load creep tests the stress level and the time at which the samples fail is recorded and it is related to the equivalent short-term strength derived from Unconfined Compressive tests. This method, while relatively simple, neglects to consider the strain path during the long-term loading. Lajtai et al. (1991) suggested, with caution (as it depends on the different minerology and the rock type of the samples tested), that the long-term strength could be estimated to lie between 53 and 60% of the ‘short-term strength’, based on laboratory data acquired from static load tests on Lac du Bonnet granite, Beebe anorthosite and Tyndallstone limestone. The latter type of rock was observed to be more time-dependent. Lau et al. (2000) also showed, after performing static load tests on Lac du Bonnet granite and granodiorite, similar results. Paraskevopoulou et al. 2015 reported that the long-term strength of igneous rocks in dry conditions should be close to 60% of the short-term strength.

Another technique to estimate the long-term strength is determined by investigating the secondary stage (steady-state phase of creep) of the creep curve. This method assumes that the delayed failure takes place when the strains attributed to dilatancy (crack volumetric) attain a certain critical value (Lajtai and Bielus 1986) and are used to predict the transition to the tertiary creep stage. Experimental and laboratory research (Scholz 1968; Lockner and Byrlee 1980; Kranz et al. 1982, Kawada and Nagahama 2004) has shown that crack propagation can also take place during creep. Cruden (1974) showed with static fatigue tests on brittle rocks under unconfined loading conditions that a critical crack density exists at which cracks begin to

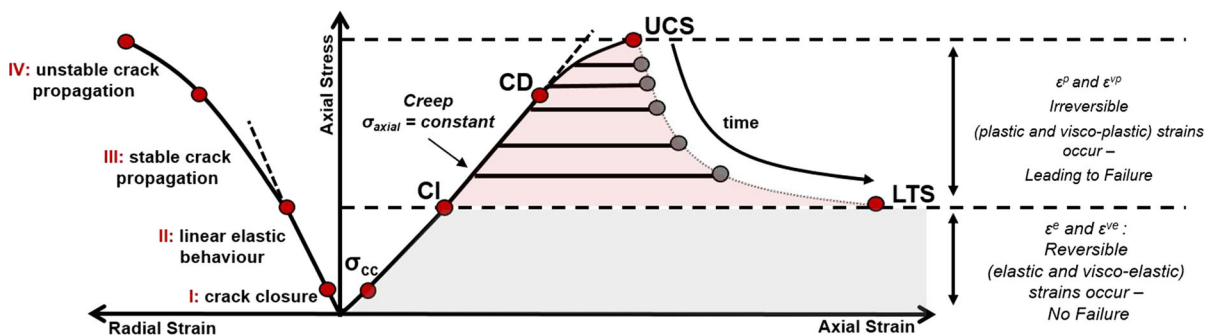


Fig. 5 Schematic representation of the stress–strain response and stages of brittle rock fracture process and evolution of the short-term strength of the material to its long-term strength when subjected to a constant stress conditions, (where: σ_{cc} stress level at crack closure, CI crack initiation, CD critical damage, UCS unconfined compressive strength, σ_c applied constant stress)

intersect. Diederichs (2003) also demonstrated this concept with statistical and numerical approaches. This crack density marks the point where accelerating crack intersection rates occur that eventually lead to failure (i.e. tertiary creep). One can then imply that time-dependent damage and delayed fracture occur and be visible under compressive loading. From the uniaxial compression and creep tests, Lajtai and Bielus (1986) concluded that the crack volume strain and its rate is a more reasonable parameter to measure crack growth in compression over time leading to delayed fracture and failure as they observed that after a short primary phase the axial strain behaves elastically with no or very little time-dependency involved. As confirmed by Diederichs (1999, 2003), a critical radial (lateral) extension strain could be related to the critical crack density of brittle rocks, associated with the onset of coalescence of cracks. In static load tests, accelerating creep rates are observed when a critical strain is exceeded.

Other methods based on reliability analysis have also been adopted to predict the long-term strength of rock materials. These methods statistically assess the reliability as the probability assuming that a material has a specific life-expectancy (time-to-failure) (Besterfield 1979). However, they require an adequate time to failure data set from static load tests. The theoretical Weibull distribution is commonly utilized, treating the data as a continuous cumulative distribution that is curve-fit to the experimental data. Lajtai et al. (1991) described in detail this method, which was applied to predict the life-expectancy on a dolomitic limestone, the Tyndallstone.

Life span estimates at the order of hundreds of years for engineering projects are based on long-term static load tests. The analysis herein presents and discusses the results of a series of static load tests on limestone to improve the capability to estimate long-term strengths in brittle rocks. The results are related to reported data available in literature as an attempt to create and establish a database to preliminary estimate the long-term strength which can be used by researchers and engineers.

3 Laboratory Testing Program and Methods

3.1 Sample Descriptions

The selected Jurassic limestone comes from a quarry north of Zurich, Switzerland, in the tabular Jura

(Fig. 6a). The samples are a fossil rich packstone, following the classification system of Dunham (1962), with variable sized vugs ranging from 0.1 to 3 mm and pyrite rich crystal patches. There are also lime-mudstone blebs ranging from 5 to 30 mm in diameter, mixed within the packstone framework. 56.0 mm diameter samples were cored from a block measuring $500 \times 500 \times 150$ mm, such that the cores long axes (before end face grinding) were 150 mm long. All the samples were prepared according to the ISRM (1979) requirements.

The Cobourg limestone (Fig. 6b) comes from the Bowmanville quarry, near Bowmanville, Ontario, Canada. The limestone has a characteristic mottled texture, with the light gray areas being a fossil rich lime-packstone and the dark gray being argillaceous lime-mudstone. A block measuring $400 \times 400 \times 700$ mm was cored perpendicular to the irregular bedding marked by the argillaceous banding. Due to the limited volume of material for testing, not all samples were 150 mm long (before end face grinding), such that the height to diameter ratio range between 2.0 and 3.0. All other sample preparation procedures were conducted according to the ISRM (1979) requirement.

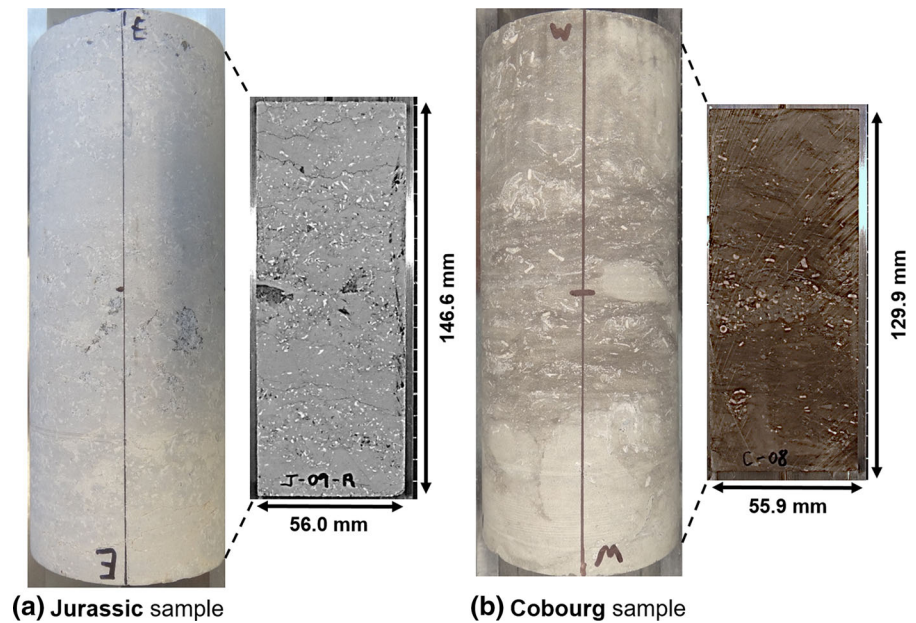
3.2 Baseline UCS Testing

A modified 2000kN Walter and Bai servo-controlled testing device was utilized to perform baseline unconfined compressive strength (UCS) testing on 19 cylindrical samples: 10 of Jurassic limestone and 9 of Cobourg limestone. A constant radial displacement rate of 0.01 mm/min was maintained during loading. A chain wrapped around the mid height of the specimen with a single strain gauge attached was used to measure the radial displacement whereas the axial strain was recorded on the sample surface by two strain gauges at the opposite sides of the specimen.

3.3 Determination of Brittle Stress Thresholds

The results from the UCS testing series were further used to determine the damage thresholds, CI, CD, and the peak strength using strain based methods, as previously described. Several methods were adopted to determine CI and CD values. CI thresholds were determined using two methods: (a) the deviation from linearity of the radial strain following on Lajtai's

Fig. 6 Samples of
a Jurassic limestone and
b Cobourg limestone



(1974) approach and, (b) the crack volumetric strain method of Martin's (1993). For CD estimation both Lajtai's (1974) deviation from linearity of the axial strain method and Beniaowski's (1967) volumetric strain reversal method were adopted. These results were used to determine the load levels for the static load testing series.

Wherever the load level was sufficient enough to identify the Crack Damage thresholds and elastic properties the loading stage (the stage prior to constant load) from the static load testing series was also used.

3.4 Static Load Testing Under Compression and Testing Procedure

The static load testing procedure presented in this paper was adopted from the ISRM (2014) suggested methods for determining the creep characteristics of rock and the ASTM (2008) guidelines for creep of rock under constant stress and temperature. During testing, relative humidity was controlled using a saturated salt solution of sodium nitrate, which should maintain a 65% relative humidity at 20 °C. Temperature was monitored in the laboratory environment which had a relatively constant climate. Overall these environmental factors were generally maintained within ± 1.0 °C and 5.0%, respectively.

The equipment used for this testing series is illustrated in Fig. 7 and consists of a manual oil pump

to apply the load. The load is held constant with the use of a hydraulic accumulator. The accumulator is filled with nitrogen gas, which acts as a spring if the oil volume changes during testing and therefore maintains the load constant. The load is applied to the sample via an expandable oil pillow with a larger diameter than the sample. The difference in area results in an approximately $2\times$ amplification of the oil pressure felt on the sample. The frames were calibrated with a load cell to determine the relationship between the oil pressure in the pillow and the load on an aluminum cylinder.

Axial and radial strains were measured using strain gauges and for some tests using the DD1 cantilever strain sensors from HBM. The DD1 sensors were damaged during initial tests on the Jurassic limestone samples and subsequently strain gauges were used on the remaining samples. Acoustic emission, both active and passive, were also measured with an Elsys TraNET EPC data acquisition system. The primary focus of this paper is on the strain evolution during the static load tests.

All tests have been performed at stress levels between CI and the peak strength. Multi-step and single-step load tests were conducted, however, the single-step tests are the primary focus of this paper. Table 1 summarizes the samples that were tested under the various conditions. Two testing series were performed for assessing the long-term creep

Fig. 7 Equipment of static loading testing with the main components labelled. The constant load is maintained with the nitrogen accumulator

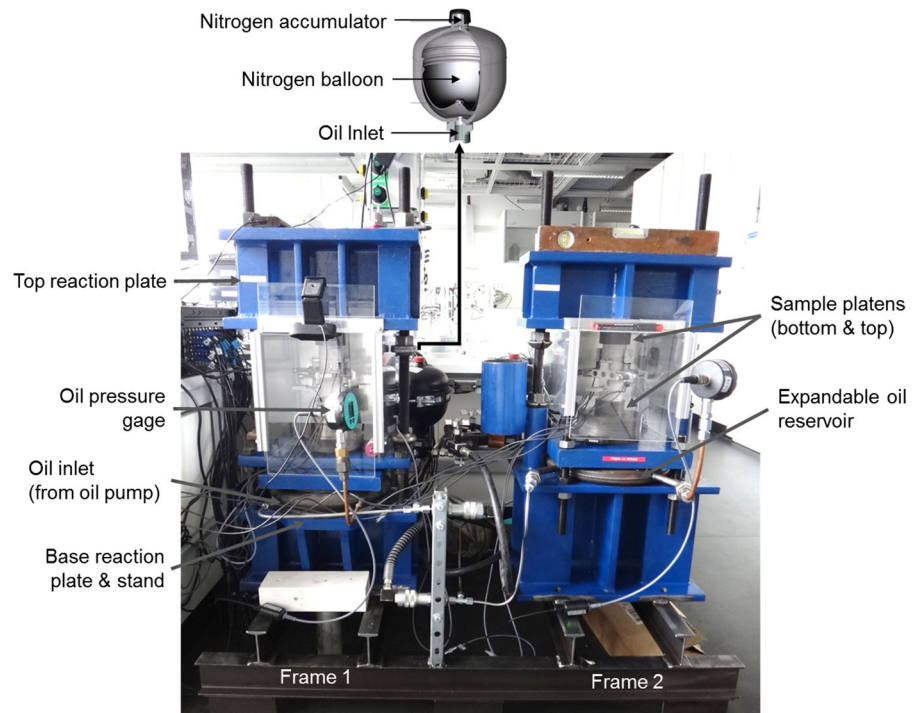


Table 1 Summary of the static-load testing types

| Rock formation | Jurassic limestone | | Cobourg limestone | |
|-------------------|--------------------|-------------------------|-------------------|-------------------------|
| Load level(s) | Single-step | Multi-step ^a | Single-step | Multi-step ^a |
| Number of samples | 10 | 2 | 4 | 1 |
| Total | 12 | | 5 | |

For each multi-step test, 10 strain levels were tested

^a Steps ranged from 2 to 4 depending on the test

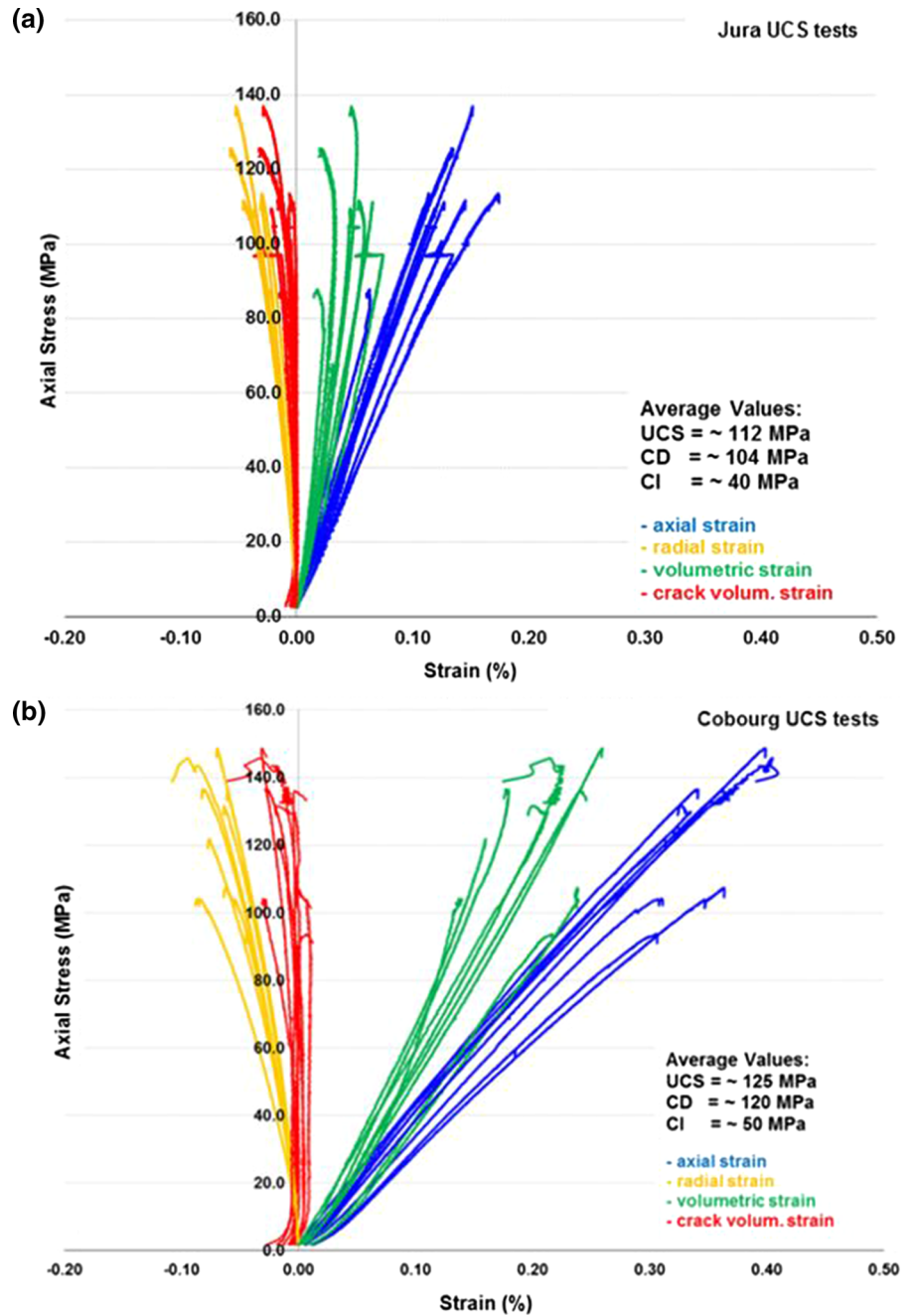
behaviour, the first was on Jurassic limestone and the second on Cobourg limestone samples.

Single-step tests were conducted on 10 Jurassic and 4 Cobourg samples and they were held at stress levels above CI (0.40 UCS) for seconds to several days until failure occurred. Most of the single-step tests fail within the first few hours and those who did not reach failure after several days to weeks were terminated and unloaded. Single-step tests are practically convenient but require more specimens to fully cover the spectrum of the expected range of the time to failure.

Multi-step tests were performed on 2 Jurassic and 1 Cobourg samples and they were conducted to compare to the single-step test stress levels. The number of steps in each test varied ranging from 2 to 4. The stress difference between the steps was decided to be 5 MPa and the duration of each step varied from 1 h up to

10 days until failure took place. The load increase was applied once the strain rate on all gauges reached a constant rate. A few Jurassic samples did not fail and it was concluded to terminate these tests and unload the samples for additional testing in the future. An advantage of the multi-step tests is that many data points, such as strain rates, at different stress levels can be attained from only one specimen. However, to examine the long-term strength and time to failure of a material the specimens need to fail under a constant load. To date there is no comparison between single-step and multi-step tests however many tests are performed using the multi-step approach when failure of the specimen is not required. Further test results from single- and multi-step tests are required to draw meaningful conclusion from a comparison. In this paper the focus is on the single-step tests and the time to failure.

Fig. 8 Stress–strain response of **a** Jurassic Samples and **b** Cobourg Samples tested in Unconfined Compressive Strength conditions



4 Laboratory Results

4.1 Baseline Testing and Damage Thresholds

The stress–strain relationships of the 10 UCS tests on the Jurassic and the 9 UCS tests on the Cobourg are shown in Fig. 8, top and bottom, respectively. The

average values estimated for UCS, CD and CI were 112, 104, 40 MPa for the Jurassic limestone and 125, 120 and 50 MPa for the Cobourg limestone, respectively. The results are summarized in Table 7 (see “Appendix”). The crack damage thresholds and peak strength were used to determine the load levels for the static load tests.

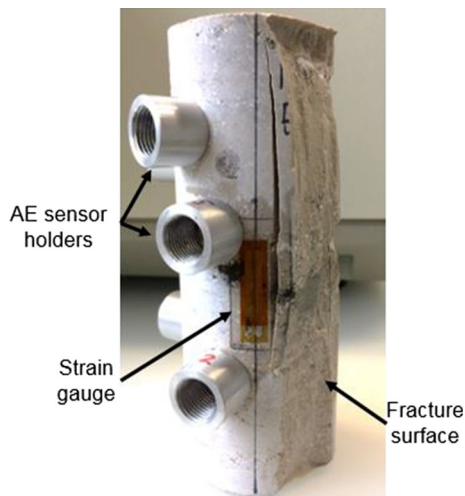


Fig. 9 An example of an axial splitting and slabbing failure mechanisms on a sample loaded near the CD threshold. The sample failed after ~ 47 min of constant loading. A strain gauge and acoustic emission (AE) sensor holders (threaded aluminium tubes) are shown on the sample surface. AE analysis is subject of a separate study

4.2 Static Load Testing

The static load testing began at load levels close to the peak strength, based on the baseline test results. Subsequent tests were conducted at lower driving stress levels approaching CD and below. In these tests, the target constant stress is applied and maintained by controlling the axial load while measuring the strains (axial and lateral) as they increase as the sample proceeds to failure Fig. 9. Samples loaded close to the peak strength fail catastrophically into many fragments, while samples loaded closer to CD fail in a less violent manner. An example of a failed sample, Jura 5S shown in Fig. 9 which failed after 2871 s at a driving stress of $0.87UCS$, shows an axial splitting and slabbing mechanism. Selective results are presented in this section, serving as examples, to describe the main influencing factors during the creep process of the two rock types.

The change in the strains over time of two single-step tests results are illustrated in Fig. 10a, b serving as examples for the Jurassic and the Cobourg limestone, respectively. The three stages of creep that a specimen of Jurassic limestone exhibited during static load testing are shown in Fig. 10a, where it is observed that radial strain on this sample is more prone to change than the axial. The transition from the secondary to tertiary stage of creep is not clearly defined as failure occurred

suddenly. It should be stated that strains were measured using the DD1 cantilever strain sensors from HBM on this sample. In the case of Cobourg limestone, Fig. 10b shows the test results of a specimen that failed some seconds after loading. In this example, the specimen has not clearly undergone the secondary stage of creep as failure occurred rapidly after reaching the load target. This causes an overlap in the creep stages, making it difficult to distinguish them clearly. For all the Cobourg samples, the strains were measured with strain gauges.

The phenomenon of failing in a few seconds after loading was observed on both types of limestone but more often in the case of the Cobourg limestone. The latter was observed on the samples loaded at stress levels above and close to the CD stress threshold and generally the time to failure increased as the driving stress decreased.

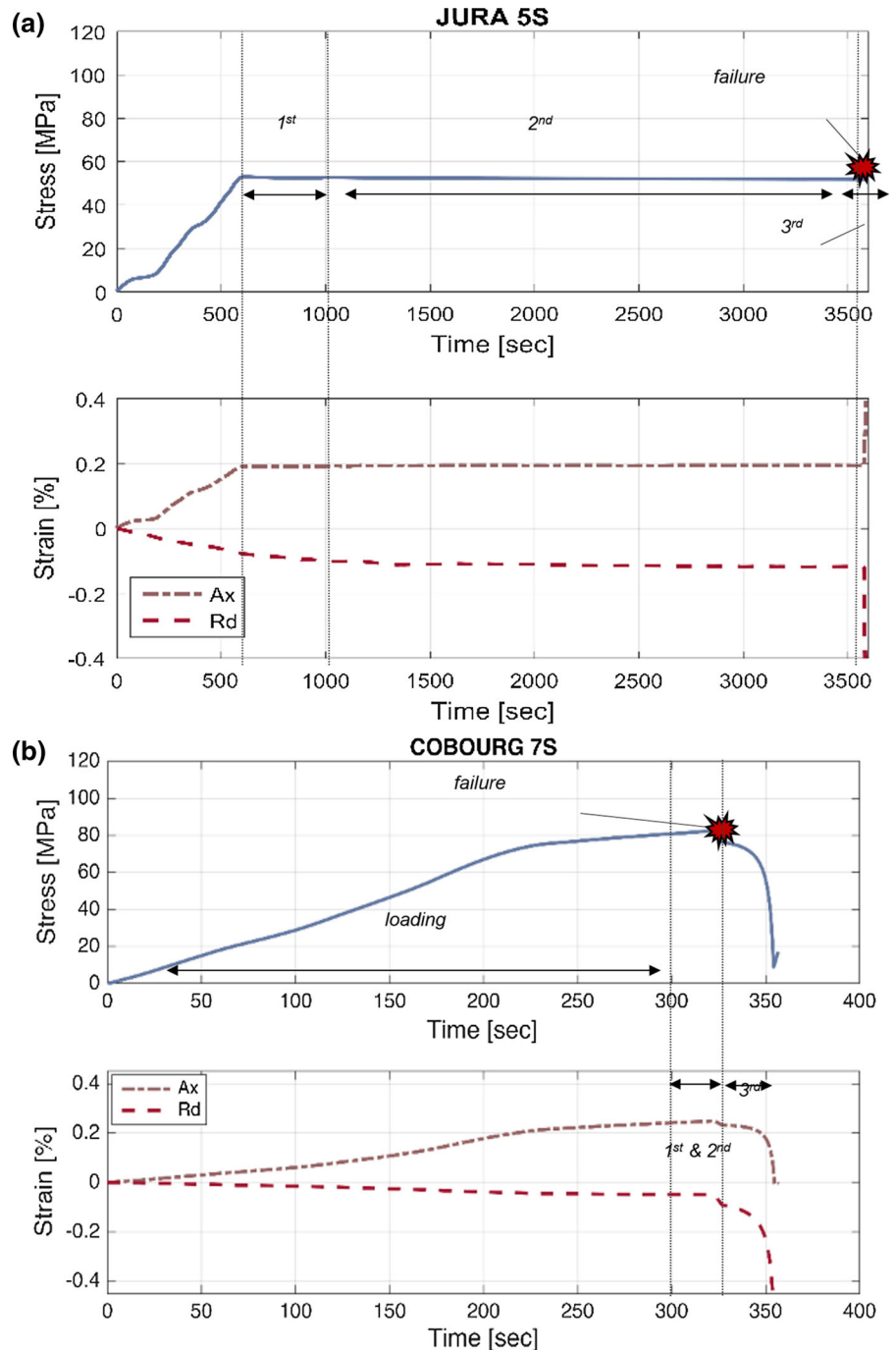
4.3 Effect of Temperature and Humidity

Temperature and humidity changes are known to cause changes in the volume of rock samples and strain rates of limestone and other rocks (Harvey 1967; Pimienta et al. 2014). Both temperature and the humidity were recorded during the testing to verify if anomalous strain readings or changes in the strain rates were the result of temperature or humidity perturbations. The stress and the strain response to temperature and humidity change during a single-step test on a Jurassic limestone sample and a multi-step test on a Cobourg limestone sample are presented in Figs. 11 and 12, respectively.

In Fig. 11a, b the stress, from the start of the loading phase up to the end of the first constant load phase, is shown with the temperature (Fig. 11a) and relative humidity (Fig. 11b) fluctuations throughout the test. The initial decrease in the temperature and increase in humidity is caused by the test chamber and the sensor re-acclimatizing after insertion of the sample and the sensor into the test chamber. The influence of this re-acclimatization phase on the volumetric strain (Fig. 11c, d) is negligible, as there is only a small drop in the stress of 1 MPa, which then stabilizes.

In the example of the Cobourg 8S sample the second-load phase (Fig. 12a, b) is shown of this multi-step test along with the volumetric strain response (Fig. 12c, d), temperature and relative humidity. The load remains exactly at the target threshold and there is only a small volumetric strain increase within the first 3 h of this load

Fig. 10 **a** Single-step static load test results of specimen ‘JURA 5S’ (Jurassic limestone). And **b** ‘Cobourg 7S’ (Cobourg limestone) Axial stress (blue line), axial strain (brown line - ‘Ax’) and radial strain (red line - ‘Rd’) results in relation to constant load time expressed in seconds. ‘1st’, ‘2nd’, ‘3rd’ denotes the primary, secondary and tertiary stage of creep behaviour observed during testing the specimens

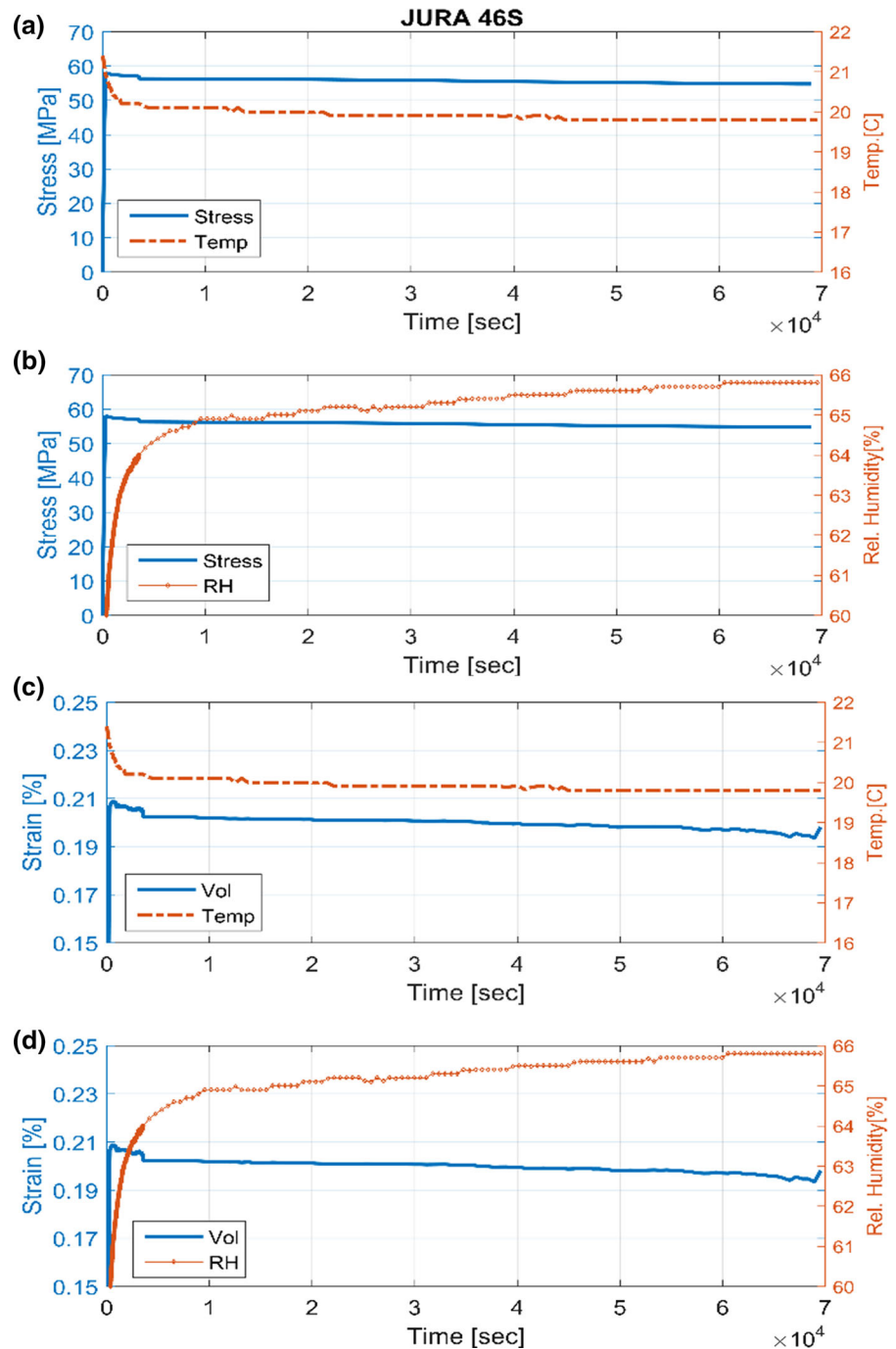


phase. This increase in volumetric strain is attributed to creep of the sample, as the temperature remains almost constant and there is a small drop in the relative humidity (<1%) in the same time period of the strain increase.

The samples (JURA 46S and COBOURG_8S) presented herein were selected as examples to show

the magnitude of the change in the laboratory conditions during static load testing and to demonstrate that within this range there is a negligible impact on both types of limestone behaviour with respect to the magnitude of the creep strains. This is clearly shown in Figs. 11 and 12c, d where the

Fig. 11 **a** Axial stress response of 'JURA 46S' sample to temperature ('Temp') and **b** relative humidity ('RH') fluctuations during single-step static load testing, **c** Volumetric strain ('Vol') response of 'JURA 46S' sample to temperature ('Temp') and **d** relative humidity ('RH') fluctuations during single-step static load testing

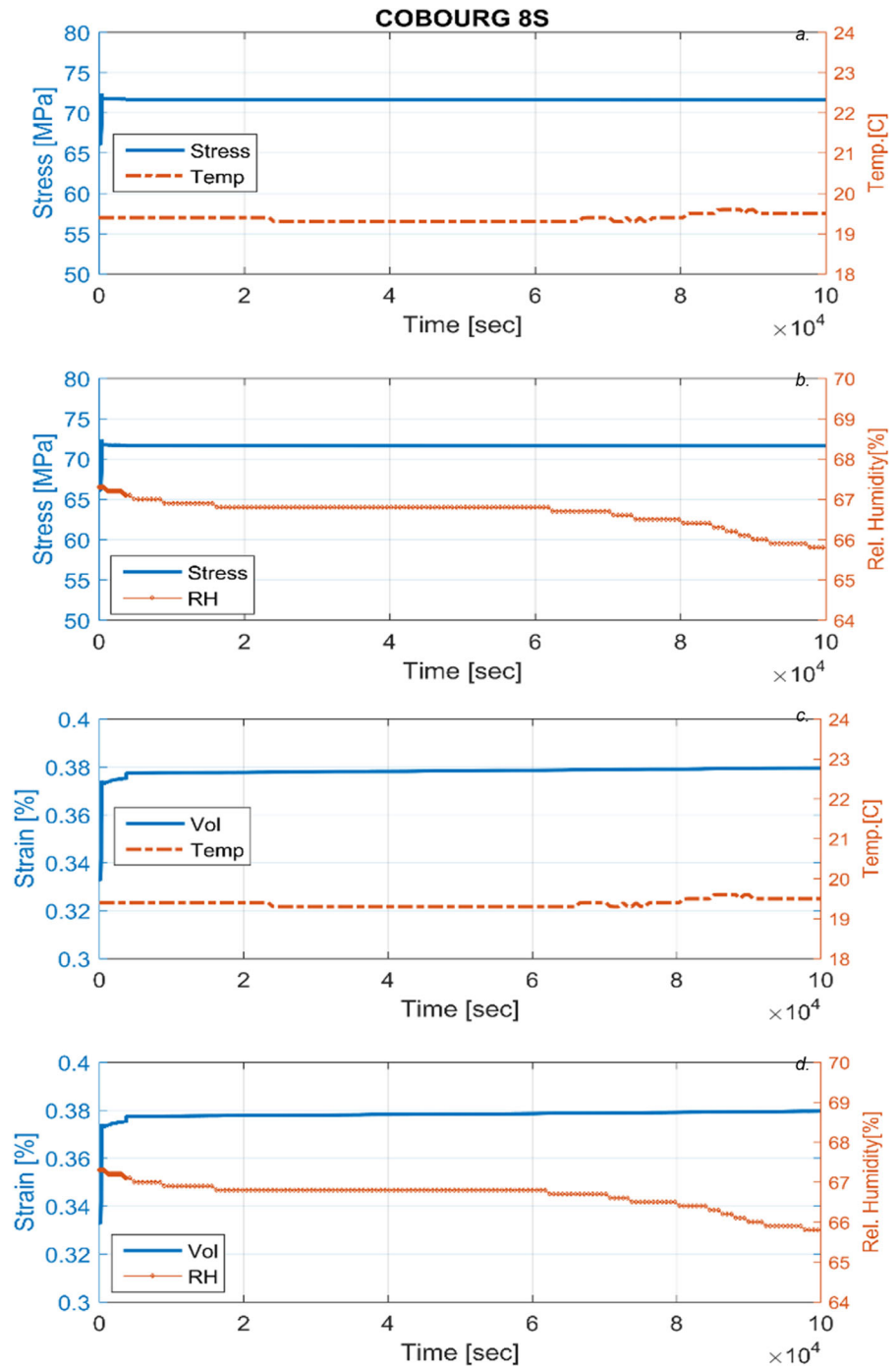


change in volumetric strain in relation to the change of temperature and humidity is presented and in both cases the volumetric strain remains relatively constant until the end of the current constant load phase.

5 Analysis and Discussion

The examination of the results presented were further analysed in order to investigate more closely the rock's response under static load conditions. Two

Fig. 12 **a** Axial stress response of ‘COBOURG 8S’ sample to temperature (‘Temp’) and **b** relative humidity (‘RH’) fluctuations during single-step static load testing, **c** Volumetric strain (‘Vol’) response of ‘COBOURG 8S’ sample to temperature (‘Temp’) and **d** relative humidity (‘RH’) fluctuations during the second step of a multi-step static load testing



aspects of time-dependency were further examined: the first aimed to estimate and derive creep parameters that can be further used in the visco-elastic Burgers model or related models and the second closely to examine the time during which the material is subjected to a static load until failure is reached.

5.1 Visco-Elastic (Creep) Parameters

The visco-elastic parameters were estimated for every sample tested, including those that did not fail. Since the visco-elastic parameters, which were used to simulate creep behaviour using the Burgers model, can

Table 2 Visco-elastic (creep) parameters for Jurassic and Cobourg limestone

| Geological formation | Sample name | Test-method used | G_K (Pa) | G_M (Pa) | η_K (Pa s) | η_M (Pa s) | Creep stress (MPa) | Driving stress-ratio (σ/UCS) | Status (failure/no failure) |
|----------------------|------------------------------|------------------|------------|------------|-----------------|-----------------|--------------------|---------------------------------------|-----------------------------|
| Jurassic limestone | <i>JURA_4S-1^a</i> | Lab | 7.55E+08 | 1.18E+07 | 9.70E+21 | 1.00E+13 | 89 | 0.64 | NF |
| | <i>JURA_4S-2^a</i> | Lab | 7.55E+08 | 1.18E+07 | 9.70E+21 | 1.00E+15 | 101 | 0.73 | F |
| | <i>JURA_5S</i> | Lab | 4.80E+08 | 1.05E+07 | 1.73E+19 | 1.74E+15 | 72 | 0.87 | F |
| | <i>JURA_6S</i> | Lab | 6.04E+08 | 3.46E+07 | 3.11E+20 | 4.12E+13 | 93 | 0.70 | NF |
| | <i>JURA_8S</i> | Lab | 3.34E+08 | 6.79E+06 | 2.98E+20 | 6.59E+13 | 91 | 0.70 | NF |
| | <i>JURA_9S-1^a</i> | Lab | 8.07E+08 | 3.54E+07 | 3.33E+21 | 2.49E+14 | 71 | 0.61 | NF |
| | <i>JURA_9S-2^a</i> | Lab | 8.07E+08 | 3.54E+07 | 3.33E+21 | 2.49E+14 | 73 | 0.62 | NF |
| | <i>JURA_37S</i> | Lab | 3.36E+08 | 2.00E+07 | 9.12E+20 | 1.38E+14 | 79 | 0.65 | NF |
| | <i>JURA_38S</i> | Lab | 1.19E+10 | 9.18E+06 | 4.58E+21 | 2.81E+12 | 65 | 0.53 | NF |
| | <i>JURA_42S</i> | Lab | 6.87E+08 | 1.85E+07 | 2.36E+19 | 2.74E+12 | 87 | 0.63 | NF |
| | <i>JURA_43S</i> | Lab | 4.80E+08 | 8.57E+06 | 9.61E+18 | 1.47E+12 | 74 | 0.49 | NF |
| | <i>JURA_44S</i> | Lab | 4.08E+08 | 3.98E+06 | 9.70E+21 | 1.64E+15 | 52 | 0.81 | F |
| | <i>JURA_45S</i> | Lab | 3.18E+09 | 3.98E+06 | 1.73E+19 | 9.02E+14 | 87 | 0.93 | F |
| | <i>JURA_46S</i> | Lab | 3.08E+09 | 3.98E+06 | 1.09E+22 | 4.75E+13 | 58 | 0.62 | NF |
| Cobourg limestone | Cobourg_5S | Lab | 1.85E+08 | 2.00E+08 | 4.53E+15 | 1.91E+15 | 66 | 0.84 | F |
| | Cobourg_7S | Lab | 2.05E+08 | 1.90E+08 | 1.53E+16 | 1.88E+15 | 82 | 0.96 | F |
| | Cobourg_8S-1 ^a | Lab | 2.04E+10 | 1.49E+08 | 1.96E+17 | 4.79E+13 | 66 | 0.65 | NF |
| | Cobourg_8S-2 ^a | Lab | 5.18E+08 | 1.66E+08 | 1.53E+16 | 1.78E+14 | 72 | 0.71 | NF |
| | Cobourg_8S-3 ^a | Lab | 2.65E+08 | 2.16E+08 | 4.46E+15 | 4.79E+13 | 77 | 0.76 | NF |
| | Cobourg_8S-4 ^a | Lab | 2.65E+08 | 2.16E+08 | 4.46E+15 | 1.78E+15 | 85 | 0.84 | F |
| | Cobourg_9S | Lab | 2.20E+08 | 1.50E+09 | 1.78E+15 | 8.36E+14 | 73 | 0.88 | F |
| Cobourg_12S | Lab | 2.26E+08 | 2.74E+09 | 5.20E+15 | 7.13E+14 | 75 | 0.96 | F | |

^a Multi-step tests

be derived from the response of the sample immediately after the loading phase, where the stress is kept constant and the sample enters the primary stage of creep and from the secondary stage of creep behaviour where the strain-rate has a constant value, the sample need not to fail in order to determine the visco-elastic properties. These properties are considered properties of the rock. The Kelvin shear modulus, G_K , the Maxwell shear modulus, G_M , the Kelvin viscosity, η_K , and the Maxwell viscosity, η_M , were estimated for the 12 tests on Jurassic limestone and for 3 of the Cobourg limestone samples, including for single-step and multi-step tests (Table 2). The Kelvin parameters refer to the delayed elastic strain response, G_K controls the amount of elastic strain and η_K the rate. The Maxwell parameters G_M and η_M are the elastic shear modulus and viscosity, respectively, and together determine the rate of viscous flow.

Goodman's approach (1980) was adopted to derive the parameters, which assume that the rock material behaves as a Burgers model according to Eq. 1, described in Sect. 2.3.1. An illustrative example of the procedure undertaken is shown in Fig. 13 and refers to the first step of the multi-step static load test performed on a specimen of the Cobourg limestone. Even in the tests that did not reach failure the creep parameters were estimated, as the Burgers model represents the primary and secondary stages of creep only and fails to capture the tertiary stage of creep.

As it has already been reported, the estimation of creep parameters is based on fitting the Burgers model to the experimental data. This can be done by drawing the asymptotic line with a slope of $(\frac{\sigma_1}{3\eta_2})$ of the constant strain rate phase or secondary creep stage and projecting back to time zero (Fig. 13). Based on this asymptote the axial strain (ϵ_B) at infinity due to time-

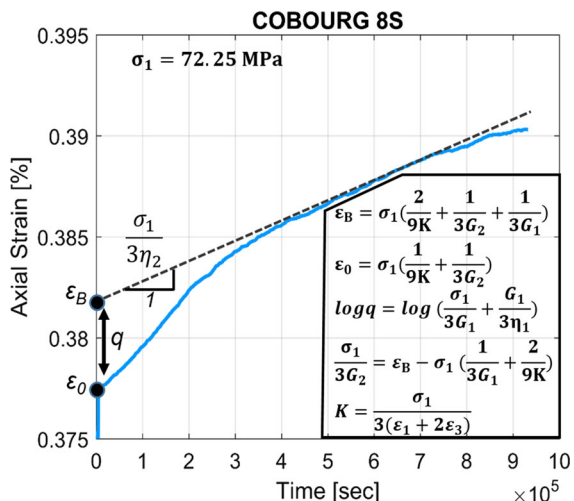


Fig. 13 Example to illustrate the estimation of the visco-elastic parameters for Burgers creep model on the first step of a multi-step static load test of a Cobourg limestone sample. The number next to ‘COBOURG’ denotes the samples name, ‘S’ refers to static load. Where: ϵ_1 is the axial strain, ϵ_3 is the radial strain, σ_1 is the constant axial stress, K is the bulk modulus, η_1 refers to η_K , Kelvin’s model viscosity, η_2 is η_M , Maxwell’s model viscosity, G_1 is G_K which is Kelvin’s shear modulus, G_2 is G_M , Maxwell’s shear modulus. ϵ_0 is the axial strain at time zero when the axial stress begins to be held constant and ϵ_B is the axial strain attained at infinity due to time-dependency

dependent deformation can be estimated as the intercept with the strain axes. Knowing from the experimental data the value of the axial strain (ϵ_0) at time = 0 (when the load is kept constant) and the value of the axial strain (ϵ_B) at infinity along with the constant stress value (σ_1) where the load is kept, the equations in Fig. 13 can be solved for the visco-elastic parameters. More specifically, (η_2) can be calculated by graphically by the slope of the asymptotic line to the secondary creep curve. Assuming that (q) is the positive distance between the creep curve and the line asymptotic to the secondary creep curve and plotting the semilog of (q) against the time (using the equation $\log q$ shown on Fig. 13) which has intercept of $(\frac{\sigma_1}{3G_1})$ and slope $(-\frac{G_1}{2.3\eta_1})$ G_1 and η_1 can be estimated. Knowing the bulk modulus (K) and using the equation for $(\frac{\sigma_1}{3G_2})$, provided on Fig. 13, G_2 can be estimated.

In this test the load was held constant at a stress level 72.25 MPa and it was held for 10.7 days. The visco-elastic parameters from this test are listed in Table 2, along with the results from the other samples tested for this study.

The visco-elastic properties from this study are compared with other limestones and other sedimentary rock types in Table 3. These have been categorized according to main rock types. Due to the challenge of finding a summary of visco-elastic parameters in the literature, Table 3 was expanded to include many other rock types. This can serve as a preliminary database that would help other researchers to easily find and further use visco-elastic parameters. The following Tables 3, 4 and 5 group the visco-elastic parameters into sedimentary, metamorphic and igneous rocks, respectively. Table 6 presents data that were applied in more complex geological systems involving two or more geological formations. Although, there is a wide range of a data available regarding visco-elastic parameters for sedimentary rocks, the data relating to time to failure are limited.

5.2 Time to Failure

Specimens of crystalline rock subjected to creep tests are found to collapse after a period of time depending on the load applied to the sample (Damjanac and Fairhurst 2010). The main focus of this study is to examine the long-term behaviour of the two types of limestone (Jurassic and Cobourg) and also investigate if a stress threshold does exist below which the rock will cease to fail. For this reason, this section is focused on analyzing and comparing the data from this testing series to other data available in literature.

In creep tests reported in the literature the loading stage of the test is rarely discussed or presented. During the loading phase, however, properties of the sample can be determined, such as the stiffness or the damage thresholds. In general the steps of the analysis procedure undertaken were the following:

- the maximum stress value at which the axial load was held constant, was recorded,
- the initial loading portion of the stress–strain curve was used and further analyzed to estimate CI stress thresholds,
- the loading rate was similar for all the tests and depending on the instantaneous stress level the initial loading duration ranged from 5 to 10 min (achieving strain-rates of 0.02–0.04 mm/min), to confirm with the ISRM suggested method of compression testing (ISRM 1979),

Table 3 Visco-elastic (creep) parameters for sedimentary rocks

| Rock type | Class | Geological formation or deposits | Test-method used | G_K (Pa) | G_M (Pa) | η_K (Pa s) | η_M (Pa s) | References | Comments |
|-------------|---------|----------------------------------|-----------------------|------------|------------|-----------------|-----------------|----------------------------------|--|
| Sedimentary | Clastic | Conglomerate | Lab | 5.92E+04 | 1.92E+05 | 2.14E+06 | 2.95E+07 | Fifer Bizjak and Zupancic (2009) | Landslide gravel material (= 50%) |
| | | Tar sand | Lab | 1.53E+05 | 1.11E+06 | 5.02E+06 | 1.30E+09 | | Landslide gravel material (= 40%) |
| | | | Lab | 1.30E+09 | 4.33E+08 | 6.67E+11 | 3.30E+13 | Rahman et al. (1992) | Partially consolidated sandstone |
| | | | Lab | 1.30E+09 | 5.33E+08 | 9.33E+11 | 3.30E+13 | | |
| | | | Lab | 2.33E+09 | 3.33E+08 | 1.83E+12 | 1.70E+13 | | |
| | | | Lab | 1.30E+09 | 6.05E+08 | 6.67E+11 | 3.30E+13 | | |
| | | | Lab | 1.30E+09 | 7.44E+08 | 9.33E+12 | 2.50E+13 | | |
| | | Sandstone | Lab | 3.24E+10 | 3.88E+09 | 6.45E+15 | 5.10E+16 | | |
| | | | Lab | 7.46E+10 | 4.02E+09 | 9.53E+15 | 2.94E+16 | | |
| | | | Lab | 4.29E+10 | 3.88E+09 | 6.59E+15 | 2.75E+16 | | |
| | | | Lab | 9.60E+09 | 2.16E+09 | 2.27E+15 | 7.48E+15 | | |
| | | Sandstone | Lab | 5.23E+11 | 6.50E+09 | 1.56E+16 | 1.51E+17 | Wei-ya et al. (2011) | High to medium coarse texture |
| | | Sandstone | Lab | 5.23E+11 | 7.55E+09 | 1.56E+16 | 1.51E+17 | | With thin-layered mudston |
| | | Sandstone | Lab | 5.23E+11 | 7.65E+09 | 1.56E+16 | 1.51E+17 | | With thin-layered siltstone and silty mudstone |
| | | Sandstone | Lab | 5.23E+11 | 7.21E+09 | 1.56E+16 | 1.51E+17 | | Thin-layered siltstone, silty mudstone and coal streak |
| | | Sandstone | Lab | 4.90E+10 | 1.47E+09 | 8.64E+14 | 1.38E+16 | | With thin-layered siltstone, silty mudstone and mudstone |
| | | Sandstone | Lab | 4.90E+10 | 3.23E+09 | 8.64E+14 | 1.38E+16 | | With pelitic siltstone |
| | | Silty mudstone | Lab | 4.90E+10 | 3.25E+09 | 8.64E+14 | 1.38E+16 | | |
| | | Mudstone and siltstone | Lab | 4.90E+10 | 2.02E+09 | 8.64E+14 | 1.38E+16 | | |
| | | Mudstone | Lab | 9.60E+09 | 2.16E+09 | 2.27E+15 | 7.48E+15 | | |
| | | | Lab | 9.50E+09 | 2.84E+09 | 1.12E+15 | 6.73E+15 | | |
| | | Claystone | Numerical simulations | 3.49E+08 | 6.67E+07 | 6.35E+14 | 4.23E+15 | Zhifa et al. (2001) | |
| | | | In situ | - | 1.36E+08 | - | 4.80E+13 | | |
| | | | In situ | - | 7.63E+07 | - | 3.73E+13 | | |
| | | | In situ | - | 6.37E+07 | - | 2.86E+13 | | |
| | | | In situ | - | 1.24E+08 | - | 7.12E+13 | | |

Table 3 continued

| Rock type | Class | Geological formation or deposits | Test-method used | G_K (Pa) | G_M (Pa) | η_K (Pa s) | η_M (Pa s) | References | Comments |
|-------------|-------|----------------------------------|-----------------------|------------|------------|-----------------|-----------------|-------------------------------|--|
| Non-clastic | | Clay shales | In situ | 8.18E+08 | 1.86E+08 | 2.10E+13 | 9.21E+13 | Chin and Rogers (1987) | |
| | | Clay shales | Lab | 3.07E+07 | 1.92E+07 | 4.47E+12 | 1.76E+14 | Bomini et al. (2009) | |
| | | Shale | In situ | 3.07E+07 | 4.00E+06 | 4.47E+12 | 2.00E+17 | | |
| | | | Lab | 3.50E+08 | 3.50E+09 | 4.20E+18 | 2.10E+16 | Sharifzadeh et al. (2013) | |
| | | Celadon argillaceous rock | Lab | 1.31E+09 | 4.10E+08 | 1.14E+15 | 1.06E+13 | Feng et al. (2006) | Sand and marine shales of Hanjiadian group |
| | | | Numerical simulations | 1.53E+09 | 6.10E+08 | 2.89E+15 | 1.15E+14 | | |
| | | Fuchsia argillaceous rock | Lab | 3.29E+09 | 2.17E+09 | 1.49E+13 | 3.60E+15 | | |
| | | Argillaceous rock | Lab | 9.80E+10 | 2.36E+09 | 8.64E+14 | 1.30E+16 | Wei-ya et al. (2011) | Sand and Marine shales of Hanjiadian group |
| | | Indiana limestone | Lab | 1.99E+11 | 1.45E+10 | 9.65E+09 | – | Hardy et al. (1970) | With broken interlayers |
| | | | Lab | 1.59E+11 | 1.72E+10 | 8.25E+09 | 2.44E+11 | | |
| | | | Lab | 1.11E+11 | 1.59E+10 | 6.61E+09 | 1.87E+11 | | |
| | | | Lab | 9.38E+10 | 1.52E+10 | 5.30E+09 | 7.35E+10 | | |
| | | | Lab | 5.38E+10 | 1.38E+10 | 3.32E+09 | 7.12E+10 | | |
| | | Limestone | In situ | 1.95E+08 | 2.20E+08 | 3.92E+13 | 5.84E+16 | Chin and Rogers (1987) | Weathered |
| | | Jurassic limestone | Lab | 7.5E+08 | 1.2E+07 | 9.7E+21 | 1.0E+15 | Paraskevopoulou et al. (2016) | |
| | | Lab | 4.8E+08 | 1.1E+07 | 1.7E+19 | 1.7E+15 | | | |
| | | Lab | 6.0E+08 | 3.5E+07 | 3.1E+20 | 4.1E+13 | | | |
| | | Lab | 6.0E+08 | 3.5E+07 | 3.1E+20 | 4.1E+13 | | | |
| | | Lab | 3.3E+08 | 6.8E+06 | 3.0E+20 | 6.6E+13 | | | |
| | | Lab | 8.1E+08 | 3.5E+07 | 3.3E+21 | 2.5E+14 | | | |
| | | Lab | 3.4E+08 | 2.0E+07 | 9.1E+20 | 1.4E+14 | | | |
| | | Lab | 1.2E+10 | 9.2E+06 | 4.6E+21 | 2.8E+12 | | | |
| | | Lab | 6.9E+08 | 1.8E+07 | 2.4E+19 | 2.7E+12 | | | |
| | | Lab | 5.0E+08 | 9.6E+06 | 9.2E+18 | 9.0E+14 | | | |
| | | Lab | 4.8E+08 | 8.6E+06 | 9.6E+18 | 1.5E+12 | | | |

Table 3 continued

| Rock type | Class | Geological formation or deposits | Test-method used | G_K (Pa) | G_M (Pa) | η_K (Pa s) | η_M (Pa s) | References | Comments |
|-----------|-------|----------------------------------|-----------------------|------------|------------|-----------------|-----------------|-------------------------------|------------|
| | | | Lab | 5.1E+08 | 7.6E+07 | 1.1E+19 | 1.6E+15 | | |
| | | | Lab | 3.1E+09 | 4.0E+06 | 1.1E+22 | 4.7E+13 | | |
| | | Cobourg limestone | Lab | 2.04E+10 | 1.49E+08 | 1.96E+17 | 4.79E+13 | Paraskevopoulou et al. (2016) | |
| | | | Lab | 5.18E+08 | 1.66E+08 | 1.53E+16 | 1.78E+14 | | |
| | | | Lab | 2.65E+08 | 2.16E+08 | 4.46E+15 | 4.79E+13 | | |
| | | | Lab | 2.20E+08 | 1.50E+09 | 1.78E+15 | 8.36E+14 | | |
| | | | Lab | 2.26E+08 | 2.74E+09 | 5.20E+15 | 7.13E+14 | | |
| | | Dolomite | In situ | 8.23E+08 | 2.98E+08 | 1.12E+14 | 4.44E+15 | Korzeniowski (1991) | |
| | | | In situ | 7.40E+08 | 2.53E+08 | 8.90E+13 | 3.98E+15 | | |
| | | | In situ | 7.62E+08 | 4.59E+08 | 7.68E+13 | 4.14E+15 | | |
| | | | In situ | 9.56E+08 | 3.08E+08 | 1.24E+14 | 4.80E+15 | | |
| | | | In situ | 7.45E+08 | 2.18E+08 | 7.63E+13 | 4.33E+15 | | |
| | | Potash | Lab | 2.00E+09 | 4.00E+09 | 6.00E+11 | 2.40E+14 | Minkley et al. (2001) | Evaporites |
| | | Camallitic rock | Lab | 2.00E+09 | 4.00E+09 | 8.64E+14 | 3.46E+11 | | Evaporites |
| | | Rock salt | Lab | 9.10E+09 | 9.00E+08 | 6.39E+11 | 3.21E+10 | Jandakaew (2007) | Evaporites |
| | | | Lab | 9.10E+09 | 1.30E+09 | 6.65E+11 | 3.21E+10 | | Evaporites |
| | | Clauberite rock salt | Lab | 9.72E+10 | 8.09E+09 | 6.50E+14 | 2.63E+16 | Zhang et al. (2012) | Evaporites |
| | | | Lab | 1.08E+11 | 9.66E+09 | 1.44E+15 | 2.44E+16 | | Evaporites |
| | | | Lab | 3.53E+10 | 8.95E+09 | 1.86E+15 | 1.14E+16 | | Evaporites |
| | | | Lab | 2.64E+10 | 7.20E+09 | 7.59E+14 | 5.37E+15 | | Evaporites |
| | | Anydrite rock salt | Lab | 2.14E+11 | 2.20E+10 | 1.12E+15 | 1.72E+16 | | Evaporites |
| | | | Lab | 6.73E+10 | 1.99E+10 | 1.72E+15 | 1.20E+16 | | Evaporites |
| | | | Lab | 2.39E+10 | 1.20E+10 | 5.58E+14 | 8.39E+15 | | Evaporites |
| | | | Lab | 2.19E+10 | 8.41E+09 | 1.18E+15 | 4.96E+15 | | Evaporites |
| | | Argillaceous rock salt | Lab | 9.56E+10 | 2.24E+10 | 5.54E+14 | 3.77E+16 | | Evaporites |
| | | | Lab | 1.81E+11 | 2.08E+10 | 5.98E+15 | 4.88E+16 | | Evaporites |
| | | | Lab | 2.15E+11 | 1.89E+10 | 1.24E+16 | 4.49E+16 | | Evaporites |
| | | | Lab | 6.00E+10 | 1.40E+12 | 1.62E+17 | 3.24E+15 | | Evaporites |
| | | Rock salt | Numerical simulations | 8.90E+08 | 3.55E+09 | 1.28E+15 | 1.82E+14 | Liu et al. (2016) | Evaporites |

Table 3 continued

| Rock type | Class | Geological formation or deposits | Test-method used | G_K (Pa) | G_M (Pa) | η_K (Pa s) | η_M (Pa s) | References | Comments |
|-----------|-------|----------------------------------|------------------|------------|------------|-----------------|-----------------|-----------------------|----------|
| | | Coal | In situ | 1.45E+08 | 1.86E+08 | 2.00E+08 | 1.03E+13 | Chen and Chugh (1996) | Organic |
| | | | In situ | 2.90E+08 | 3.59E+08 | 2.90E+07 | 8.28E+12 | | Organic |
| | | | In situ | 2.07E+08 | 2.55E+08 | 1.66E+07 | 5.03E+12 | | Organic |
| | | | In situ | 6.14E+08 | 1.10E+08 | 1.72E+07 | 2.62E+13 | | Organic |
| | | | In situ | 2.07E+08 | 2.07E+08 | 1.10E+08 | 6.90E+12 | | Organic |
| | | | In situ | 1.31E+09 | 2.28E+08 | 1.24E+09 | 1.38E+13 | | Organic |
| | | | In situ | 3.59E+08 | 9.66E+07 | 1.86E+08 | 1.79E+13 | | Organic |
| | | | In situ | 8.28E+06 | 4.90E+09 | 6.69E+09 | 1.52E+14 | | Organic |
| | | | In situ | 1.86E+09 | 2.14E+09 | 3.79E+08 | 4.41E+13 | | Organic |
| | | | In situ | 2.21E+09 | 3.10E+09 | 3.52E+08 | 8.28E+14 | | Organic |
| | | | In situ | 2.55E+08 | 8.28E+07 | 1.03E+11 | 3.24E+12 | | Organic |
| | | | In situ | 4.14E+07 | 5.52E+08 | 1.66E+10 | 1.03E+12 | | Organic |
| | | | In situ | 5.66E+08 | 2.41E+08 | 4.97E+10 | 2.00E+13 | | Organic |
| | | | In situ | 3.66E+08 | 4.14E+08 | 1.52E+11 | 8.28E+12 | | Organic |
| | | | Lab | 4.07E+09 | 1.38E+09 | 2.69E+12 | 6.57E+14 | | Organic |
| | | | Lab | 8.07E+09 | 3.66E+09 | 4.48E+12 | 3.14E+14 | | Organic |
| | | Chalk | Lab | 1.10E+11 | 2.00E+10 | 9.93E+14 | 5.46E+16 | Abass et al. (2006) | Organic |

Table 4 Visco-elastic (creep) parameters for metamorphic rocks

| Rock type | Class | Geological formation or deposits | Test-method used | G_K (Pa) | G_M (Pa) | η_K (Pa s) | η_M (Pa s) | References | Comments |
|-------------|-------------------|----------------------------------|------------------|------------|------------|-----------------|-----------------|----------------------|-------------------------|
| Metamorphic | Non-foliated | Quartzite | Lab | 6.00E+10 | 1.40E+12 | 1.62E+17 | 3.24E+15 | Malan et al. (1997) | |
| | | Quartzite | In situ | 1.47E+11 | 5.00E+12 | 8.28E+15 | 9.00E+14 | Malan et al. (1998) | |
| | Slightly foliated | Gneiss | Lab | 1.22E+09 | 1.22E+09 | 1.00E+20 | 1.00E+20 | Apuani et al. (2007) | |
| | | Mylonite | Lab | 6.73E+08 | 6.73E+08 | 1.00E+19 | 1.00E+19 | Apuani et al. (2007) | |
| | Foliated | Phyllite | Lab | 2.80E+10 | 1.60E+10 | 3.06E+14 | 9.00E+15 | Lu et al. (2015) | In saturated conditions |

Table 5 Visco-elastic (creep) parameters for igneous rocks

| Rock type | Class | Geological formation or deposits | Test-method used | G_K (Pa) | G_M (Pa) | η_K (Pa s) | η_M (Pa s) | References | Comments |
|-----------|----------|----------------------------------|-----------------------|------------|------------|-----------------|-----------------|------------------------|--------------------------|
| Igneous | Plutonic | Granite | In situ | 7.00E+11 | 5.10E+10 | 3.70E+14 | 9.50E+18 | | Fresh or microweathering |
| | | Granite | In situ | 2.00E+11 | 4.00E+10 | 8.50E+13 | 3.50E+17 | | Weak-weathering |
| | | Granite | In situ | 6.00E+10 | 3.00E+10 | 3.60E+13 | 8.50E+18 | | Weak-weathering |
| | | Granite | In situ | 8.00E+10 | 4.00E+10 | 7.80E+13 | 3.00E+17 | | Weathered (fault area) |
| | | Granite | In situ | 5.00E+10 | 3.00E+10 | 1.80E+13 | 8.00E+17 | | Weathered (fault area) |
| | Volcanic | Andesite | Numerical simulations | 6.00E+08 | 3.85E+08 | 5.00E+15 | 2.50E+17 | Guan et al. (2008) | Lava |
| | | | Numerical simulations | 8.00E+08 | 3.85E+08 | 5.00E+16 | 5.00E+17 | | Lava |
| | | | Numerical simulations | 4.00E+08 | 3.85E+08 | 2.50E+16 | 2.50E+17 | | Lava |
| | | Lava | Lab | 8.80E+10 | 2.10E+12 | 6.48E+17 | 1.37E+16 | Malan et al. (1997) | |
| | | Tuff | In situ | 3.39E+08 | 4.97E+08 | 2.13E+13 | 6.06E+13 | Chin and Rogers (1987) | |

- the time was set to zero at the point where the axial load was held constant, as illustrated in Figs. 4 and 5,
- the maximum stress was normalized to estimate UCS value for comparison to the literature and related to the time the sample was sustained at the same stress level,
- the maximum stress was also normalized to the CI value from each sample tests, as it is an

- independent value from the sample subject to the creep test,
- and the visco-elastic parameters were determined.

It should be stated here that each test was analyzed following the afore-scribed method. Similarly, in the case of the multi-step test this procedure was followed for each step apart from the CI estimation that was estimated

Table 6 Visco-elastic (creep) parameters for complex rockmass systems rocks

| Rock type | Class | Geological formation or deposits | Test-method used | G_K (Pa) | G_M (Pa) | η_K (Pa s) | η_M (Pa s) | References | Comments | |
|----------------------------|-------------------|---|-------------------------|------------|------------|-----------------|-----------------|-----------------------|--|--|
| Complex geological systems | Sedimentary based | Deposits and flysh | In situ | 2.50E+08 | 3.84E+08 | 2.10E+19 | 2.10E+19 | Marcato et al. (2009) | | |
| | | | Carboniferous formation | In situ | 4.98E+08 | 5.76E+08 | 1.35E+14 | 8.82E+14 | Barla et al. (2008) | Shists, sandstones, coal, clay-like shales and cataclastic rocks |
| | | | | Lab | 4.98E+08 | 5.66E+08 | 1.34E+14 | 8.82E+14 | Barla et al. (2010) | Shists, sandstones, coal, clay-like shales and cataclastic rocks |
| | | Hard sandstone, psammites, schists, shale and coal, cataclasite | In situ | 1.80E+05 | 7.60E+06 | 1.08E+15 | 1.08E+16 | Pellet (2010) | Shists, sandstones, coal, clay-like shales and cataclastic rocks | |
| | | | Numerical simulations | 2.50E+08 | 2.50E+08 | 5.40E+14 | 3.02E+15 | | | |
| | | | Numerical simulations | 2.50E+08 | 2.50E+08 | 1.08E+14 | 8.64E+14 | | | |
| | | | Numerical simulations | 2.50E+08 | 5.50E+08 | 1.90E+14 | 1.19E+15 | | | |

only in the initial loading at the beginning of the test. All the results presented refer to unconfined conditions.

5.2.1 Estimating the Crack Initiation and Driving Stress-Ratio

In the literature most of the testing results are presented in the form of time against the driving stress-ratio. The driving stress-ratio is commonly defined and used as the stress normalized by the strength of the sample, such as the UCS for unconfined creep tests. In most cases the UCS is taken as an average value from standard UCS tests and not determined on the same sample being subject to the creep test. In this section, the authors present a new solution to examine similar datasets. It should be noted

herein that the time needed to perform such tests as by definition they require time and a controlled and stable environment where no temperature and humidity fluctuations take place.

One way to avoid normalizing by an average UCS value is to use CI instead, as it is directly derived from the tested specimen from the initial loading part of each static load test. For this reason the authors decided to introduce the Crack Initiation Stress-ratio by normalizing the applied stress by the CI value measured on the sample with the values presented in Table 8 (see “Appendix”).

However, when comparing this dataset to similar tests available in literature using the Crack Initiation Stress-ratio appeared to be problematic since there is a limited amount of static load data presented with the

complete stress–strain curves from the loading of each sample. Martin et al. (1999) suggested that there is a consistent relationship between UCS and CI for brittle rocks. The authors have found this to be true for a number of test series with similar lithologies and consistent testing protocols (Perras and Diederichs 2014). Since there was little data in the literature to determine CI values directly from static load tests, the authors decided to convert the CI values from the static load tests of this study to an equivalent UCS value. For this purpose the CI and UCS values from the Baseline testing series with a strain-rate of 0.01 mm/min for the two types of limestone were used to develop the conversion factor. The relationship between the UCS and CI, shown in Fig. 14, for both limestone were used to estimate the UCS of the samples tested in the static load series. More specifically, the numbers 2.66 for Jurassic and 2.52 for Cobourg were multiplied with the CI values estimated from the loading portion of the static load test for each sample, as reported in Table 8 (see “Appendix”). The modified UCS* can be estimated using Eqs. (2) and (3):

$$UCS^* = a * CI \quad (2)$$

$$a = \frac{UCS^B}{CI^B} \quad (3)$$

where UCS* is the estimated UCS, CI is the Crack Initiation value derived from the static load test, α is a constant and describes the slope of the CI versus UCS

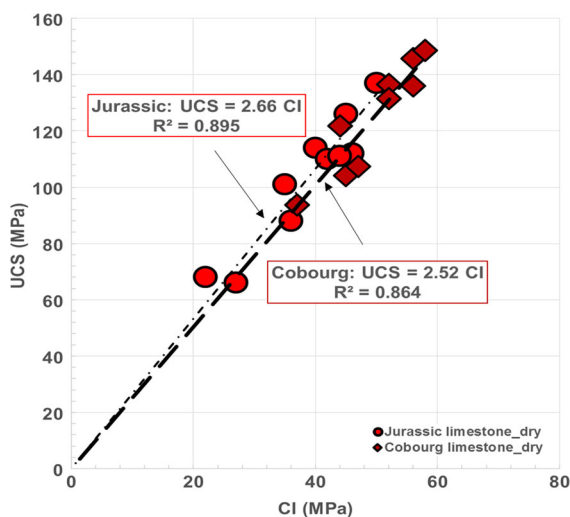


Fig. 14 The relationship between UCS and CI for the Jurassic and Cobourg limestone from the Baseline Testing

graph, and the superscript B denotes values from the Baseline Testing. This relationship was used to determine the Crack Initiation Stress-ratio for the static load tests presented in this paper.

5.3 Jurassic and Cobourg Limestone Static Load Testing Series

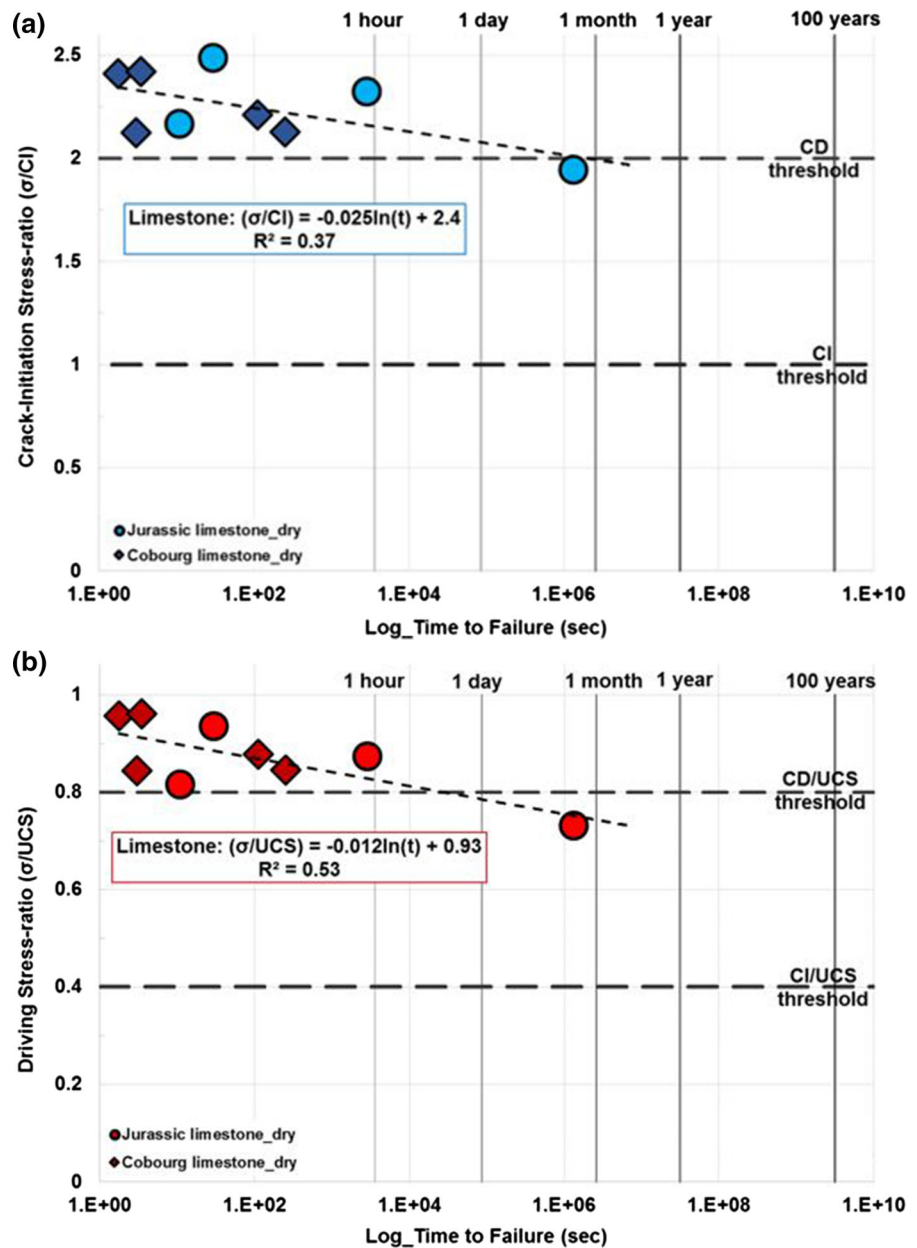
The results from laboratory testing on the two types of limestone (Jurassic and Cobourg) are presented in Fig. 15 using the Crack Initiation Stress-ratio (Fig. 15a) and the driving stress-ratio (Fig. 15b), as described in the previous section. The results refer to the samples that reached failure. All the results from the testing series including the samples that did not fail are summarized in Table 9 (see “Appendix”).

It can be observed that when the applied load is more than 0.8UCS failure takes place within an hour and when it is below or close to the CD threshold failure will occur in a longer period of time, ranging from days up to 1 month. When the data in Fig. 15b are compared with other static load test results from various rock types, the time to failure of the samples from this study seem to follow a similar trend, as shown in Fig. 16. From the data presented in this paper and that gathered from the literature, there are no samples loaded below the CI threshold which fail.

The following analysis (Figs. 17, 18, 19) examines the data set of Fig. 16 in more detail. Figure 17 categorizes the data according to the main rock type, sedimentary, metamorphic, and igneous, Fig. 18 specifically compares the limestone samples tested as part of this study with the largest time to failure data set from tests on the Lac du Bonnet granite, and Fig. 19 separates test results into dry and wet samples. The sedimentary rocks (Fig. 17a) appear to follow a similar trend with the metamorphic rocks whereas igneous rocks show more scatter. This is partly due to the fact that most time to failure test results have in the past been on igneous rocks and that there are less sedimentary and metamorphic test results. There could also be a contribution to the scatter due to different grain sizes of the mostly granite rocks tested, however, even the Lac du Bonnet data set has wide scatter in the test results. This could be explained due to the fact that igneous rocks are characterized by grain scale heterogeneity.

Granites and limestones, even though they fail in a similar manner following the principles of brittle failure theory, their long-term strength is directly

Fig. 15 Static load test data of Jurassic and Cobourg limestone, granite and granodiorite performed at room temperature in dry conditions, **a** Crack Initiation Stress-Ratio (applied initial stress normalized to CI) **b** Driving Stress-Ratio normalized to UCS*



dependent on lithology, as better shown in Fig. 18. Granitic rocks, due to heterogeneous mineralogy and their different intrinsic properties, allow different creep behaviour within different constituent crystal. As a result, ongoing creep creates mechanical conflicts resulting from the different flow-rates between the different grains leading to damage. This creep-induced damage process is less dominant in monomineralic limestones and therefore creep can occur with less weakening on the bonds between the minerals and as a

result it can sustain more deformation prior failure over longer periods of time than granite.

Nevertheless, when each rock type (sedimentary, metamorphic, or igneous) is considered as a whole, the trends for each are all similar (Fig. 19). Differences in the trend start to emerge when examining individual sample sets. This is partly because there is a lack of statistically representative data sets on an individual sample set, with perhaps the exception of the Lac du Bonnet set. For example, besides the Jurassic and

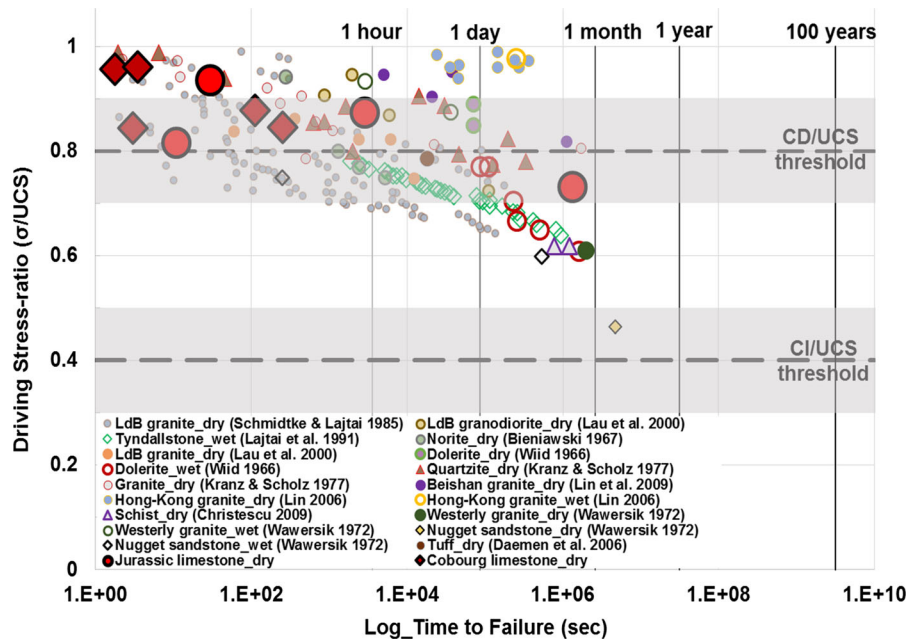


Fig. 16 Static load test data for hard rocks performed at room temperature in wet or dry conditions (where the driving stress-ratio is the stress level at failure to unconfined compressive

Cobourg limestone dataset presented in this paper, only a few more dataset were found in the literature for brittle sedimentary rocks (excluding the numerous creep studies on weak soft rocks). In contrast, for igneous rocks, the data available are more numerous, as more studies have been conducted on time to failure for granitic rocks, perhaps due to the long-standing interest in granitic rocks for the storage of nuclear waste (Perras and Diederichs 2016).

Another separation of this dataset was to examine the influence of the moisture content in the long-term strength and this is shown in Fig. 19. For the wet samples, the lowest stress at which failure occurs was at 0.6 UCS whereas in dry conditions it was closer to 0.5 UCS but this sample failed in a longer period of time. This is inverse to what is typically observed in short-term tests, where moisture tends to weaken the rock samples. However, in the long-term tests moisture content makes the samples fail within a shorter-period of time than the dry samples which in a way one can argue that moisture content does indeed make the samples weaker. The time needed for the wet samples to fail ranges from 1 h to 1 month. Widd (1966) reported that water aids the failure process and moisture affects the time-dependent aspects of the long-term strength, as moisture lowers the surface free energy in the path of the

strength of the material). CI/UCS threshold range of 30–50% (Martin et al. 1999), CD/UCS threshold range of 70–90% (Perras and Diederichs 2014)

growing cracks (Colback and Widd 1965). However, if the load is applied to the sample in with a high strain-rate, the moisture will not have time to migrate to the crack tips and will not affect the rock's strength. As Widd (1970) also reported moisture increase leads to strength reduction reflecting the primarily decrease in the molecular cohesive strength of the material. Therefore, one would anticipate that failure at a lower driving stress would be more likely for wet samples. The difference indicated in the literature data is likely more representative of the lack of test results available for comparison, rather than that dry samples can fail at lower driving stress-ratios.

The samples that did not fail are shown in Fig. 20, both from this study and from the literature. The samples closer to the CD threshold are expected to fail. They could be outliers or more likely they are stronger than the average UCS value, which is typically used to normalize the time to failure plot. Test with driving stresses below the CI threshold exhibit no failure for the duration of the test. Many of the test results with a driving stress greater than the CI threshold would be expected to fail in the time frame for which the test lasted. For the samples tested in this study, further investigation into these samples that did not fail is discussed in the next section.

Fig. 17 Static load test data for: **a** sedimentary, **b** metamorphic, **c** igneous rocks performed at room temperature in wet or dry conditions (where the driving stress-ratio is the stress level at failure to unconfined compressive strength of the material). CI/UCS threshold range of 30–50% (Martin et al. 1999), CD/UCS threshold range of 70–90% (Perras and Diederichs 2014)

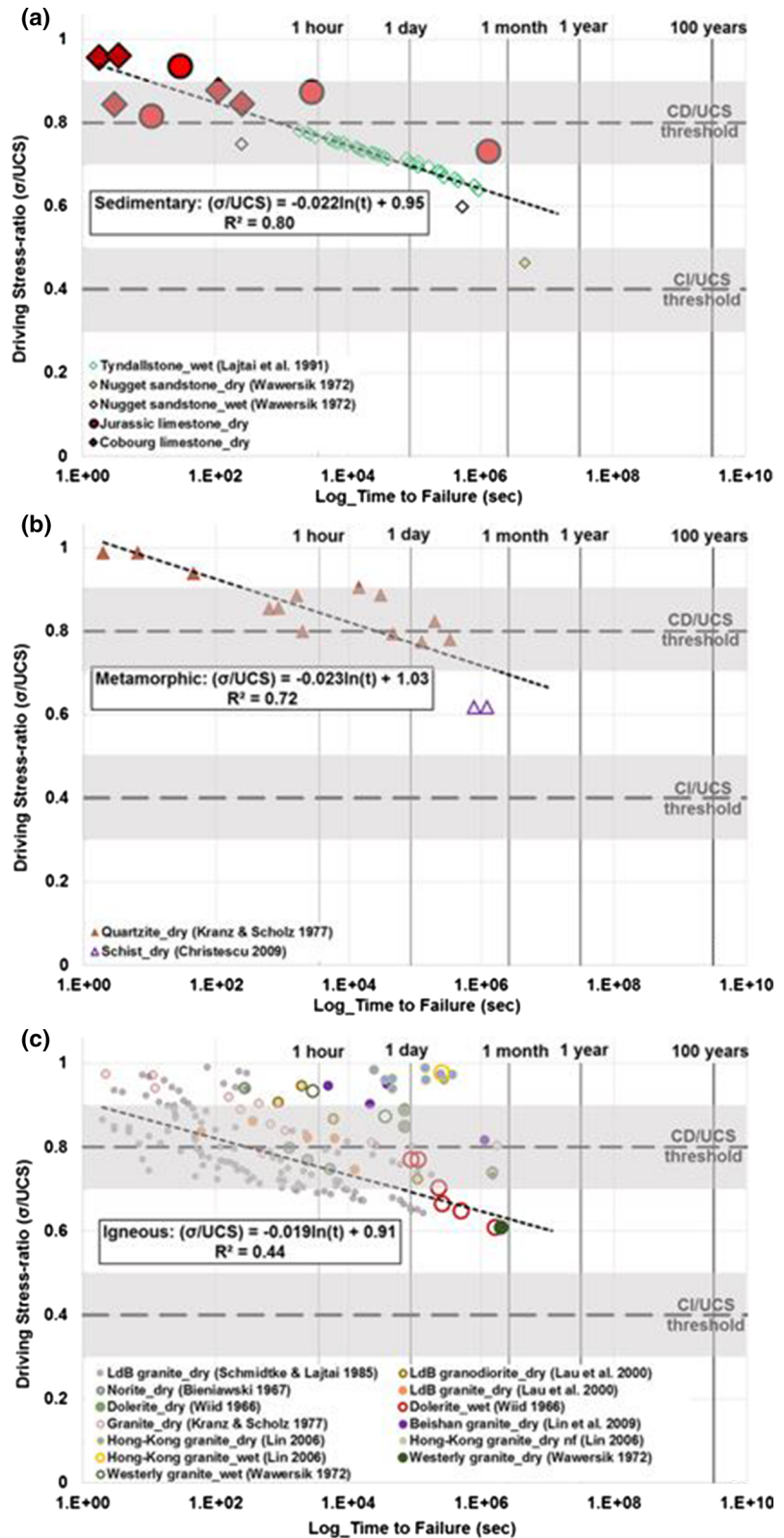
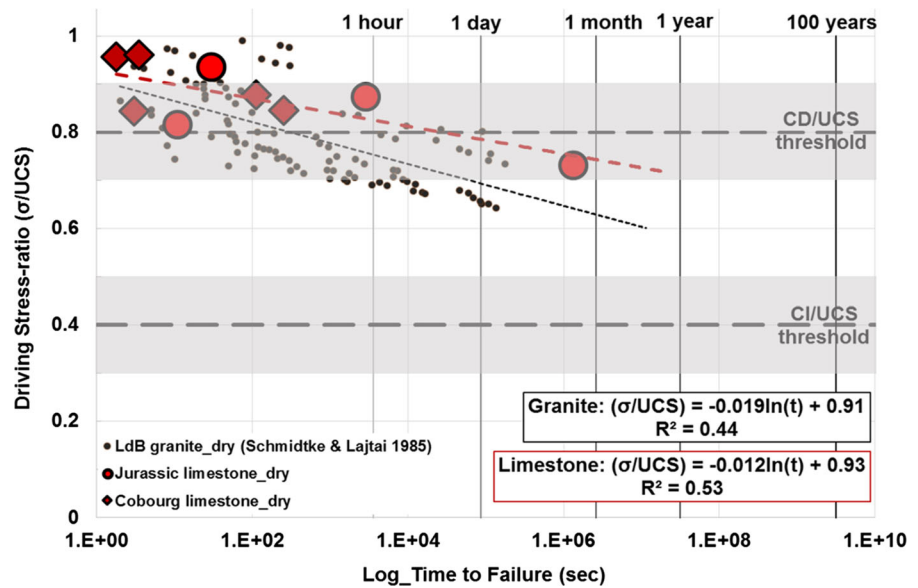


Fig. 18 Comparison of static load test data on limestone and granite performed at room temperature in dry conditions (where the driving stress-ratio is the stress level at failure to unconfined compressive strength of the material). CI/UCS threshold range of 30–50% (Martin et al. 1999), CD/UCS threshold range of 70–90% (Perras and Diederichs 2014)



5.4 Visco-Elastic Creep Parameters and Time to Failure

To examine further the reason why some samples did fail and some others not, the visco-elastic creep parameters derived from each static load test were related to time and compared to the driving-stress ratio stress-ratio. The G_K (Kelvin's shear modulus), η_K (Kelvin's model viscosity) and G_M (Maxwell's shear modulus), when plotted against time, provide no information and give no indication on why some samples failed and others did not as shown in Fig. 21. This is expected as the Kelvin model describes the delayed elasticity (the amount and the rate) and the Maxwell's shear modulus refers to the elastic shear modulus and is almost independent of the stress (Goodman 1980).

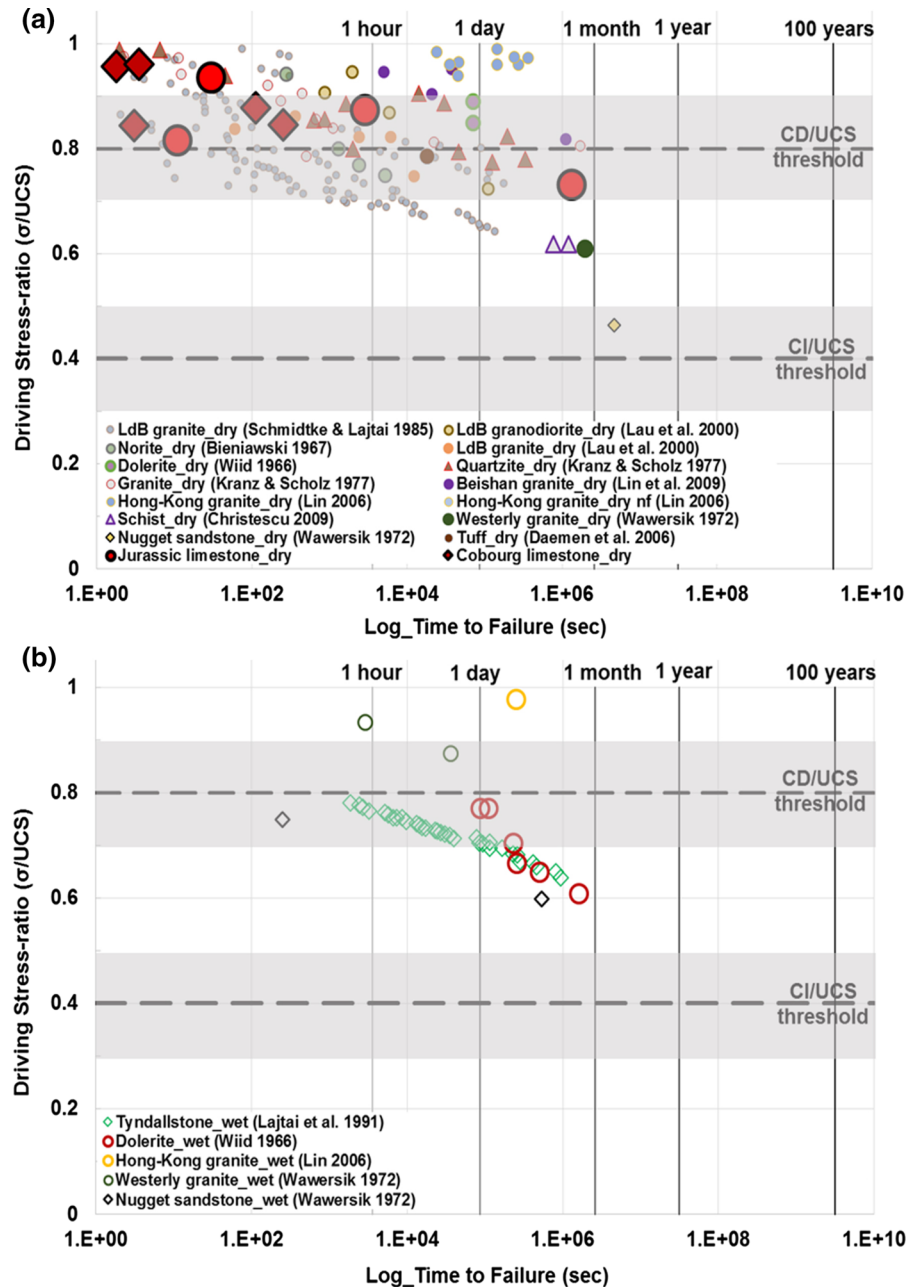
However, when the data set is compared to the viscosity of the Maxwell's model, which determines the rate of viscous flow, it shows a clear separation between samples that failed and those that did not, as shown in Fig. 22.

Viscosity is the resistance of matter to flow. The less viscous a material is, the easier it is to flow. This is in agreement with the results of this study. It is shown that the more viscous samples did reach failure (shown Fig. 22 with filled shapes) whereas the less viscous tended to creep more as they are prone to flow. It can be noted that there is a threshold in viscosity below

which the samples exhibit creep behaviour without creep leading to accumulated damage. This means that the creep behaviour can take place without damaging the rock and leading to failure.

To further understand how the above finding influences the time to failure, all results from the current testing series (failure and no failure) were further examined. Figure 23 shows the data from this testing data set for both the Jurassic and Cobourg limestone samples and some other reported data on Cobourg limestone for comparison. It is shown that above 0.8 UCS or the CD threshold all samples failed within an hour. Above the CD threshold failure occurs inevitably due to the propagation and interaction of previously formed cracks. Below the CI threshold, where pre-existing cracks are closing and elastic strains govern no failure should occur as Gorski et al. (2009, 2010) reported from testing Cobourg limestone samples for up to 100 days. Commonly, the static load levels fall between the CI and the CD thresholds (Perras and Diederichs 2014). This region is shown in Fig. 23 as an uncertain region since between CI and CD crack propagation and accumulation of damage takes place in the short-term, but in the long-term the time component can degrade the rock further leading it to failure. However, from Fig. 23, below 0.7UCS no failure is shown. These no-failure points could simply be the result of not holding the load constant long

Fig. 19 Static load test data hard rocks performed at room temperature in **a** dry and **b** wet conditions (where the driving stress-ratio is the stress level at failure to unconfined compressive strength of the material). CI/UCS threshold range of 30–50% (Martin et al. 1999), CD/UCS threshold range of 70–90% (Perras and Diederichs 2014)

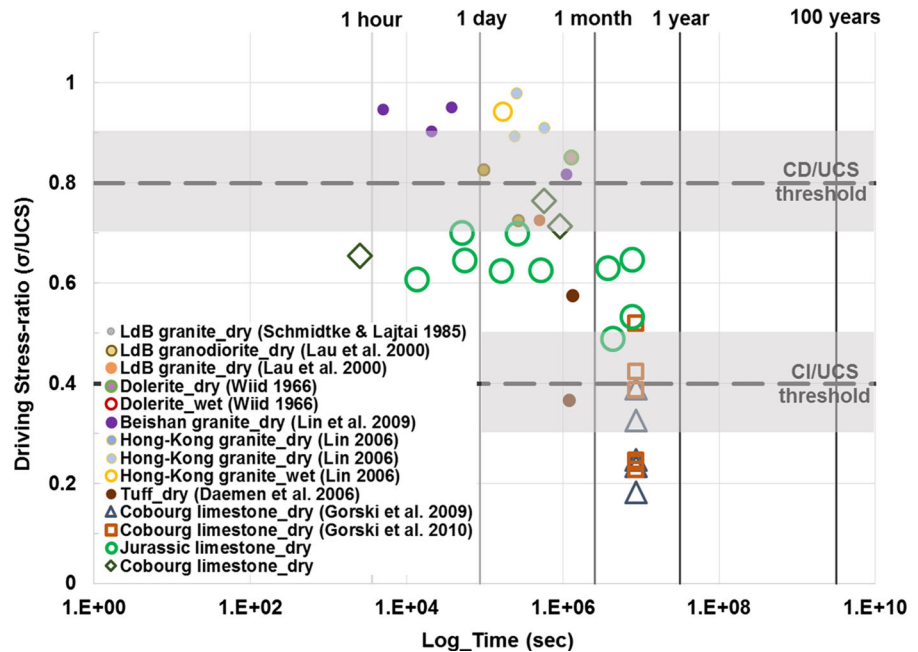


enough and therefore they would shift to the right, despite data from the literature suggesting that failure could be expected at such driving stress-ratios. Static-load tests with duration from 6 months to 1 year are suggested to examine if samples of the limestones in this study would fail at such driving stress-ratios.

Moreover, the time-dependent behaviour discussed in this paper is interpreted to be, in part, the result of

the behaviour of new microcracks, the intensity of which impacts the final UCS value (Diederichs 2003). Since the loading phase typically goes above the CI level then new microcracks should form, at least during the loading phase. Since the radial strain is increasing during static loading (Fig. 10), new microcracks are likely forming. It is perhaps possible that existing microcracks are extending.

Fig. 20 Static load test data hard rocks performed at room temperature in **a** dry and **b** wet conditions (where the driving stress-ratio is the stress level at failure to unconfined compressive strength of the material), these samples did not reach failure.). CI/UCS threshold range of 30–50% (Martin et al. 1999), CD/UCS threshold range of 70–90% (Perras and Diederichs 2014)



6 Concluding Remarks

Creep is the increase of strain at a constant load. A static load uniaxial compression test is one method of measuring deformation due to creep. This test was utilized in this study to examine a lower bound driving stress at which failure occurs and to examine the tests which did not fail under certain driving stresses.

In all tests, the axial load (stress) was kept constant throughout the test and both the axial and radial strains were recorded. In this testing series single-step and multi-step tests were conducted. Single-step tests are practically convenient but require more specimens to fully cover the spectrum of the examined behaviour. An advantage of the multi-step tests is that many data points (e.g. visco-elastic parameters) at different driving stress levels can be attained from only one specimen, however, using these tests for time to failure analysis is still subject to further analysis.

From the testing series, the visco-elastic parameters, used in Burgers model, were estimated. In addition, a large data base of visco-elastic parameters were gathered to compare with those from this study and present a useful summary of such parameter for a variety of rock types. The visco-elastic parameters from the literature have a wide range of values. Those tested in this study show a variance even in the range

of 3 orders of magnitude. Such a range, when used in numerical simulations, can result in different deformation results that can further influence the type of failure mode. In addition, it is suggested, when one may utilize the values of the visco-elastic parameters presented herein to reference the study, the type of test and the conditions undertaken.

In addition to the visco-elastic properties, the time to failure of two types of limestone, Jurassic and Cobourg samples, were examined and compared to various other rock types in the literature. The overall trend of the data from this agrees well with data from the literature and when the trends are examined by rock type the resulting fits for prediction of the time to failure of laboratory samples are as follows:

- Sedimentary: $(\sigma/UCS) = -0.022\ln(t) + 0.95$
- Metamorphic: $(\sigma/UCS) = -0.023\ln(t) + 1.03$
- Igneous: $(\sigma/UCS) = -0.019\ln(t) + 0.91$

where “t” refers to time (expressed in sec) and (σ/UCS) the driving stress-ratio, based on the trends from Fig. 17.

When the limestone data from this study is compared to the largest data set of such tests, on the Lac du Bonnet granite, the trend is shallower for the limestone. This suggests that the lower bound driving

Fig. 21 Relating **a** Time vs. Kelvin's shear modulus **b** Time vs. Kelvin's viscosity **c** Time vs. Maxwell's shear modulus. The static load test data performed at room temperature in dry or wet conditions (stress levels can be referred to Fig. 15)

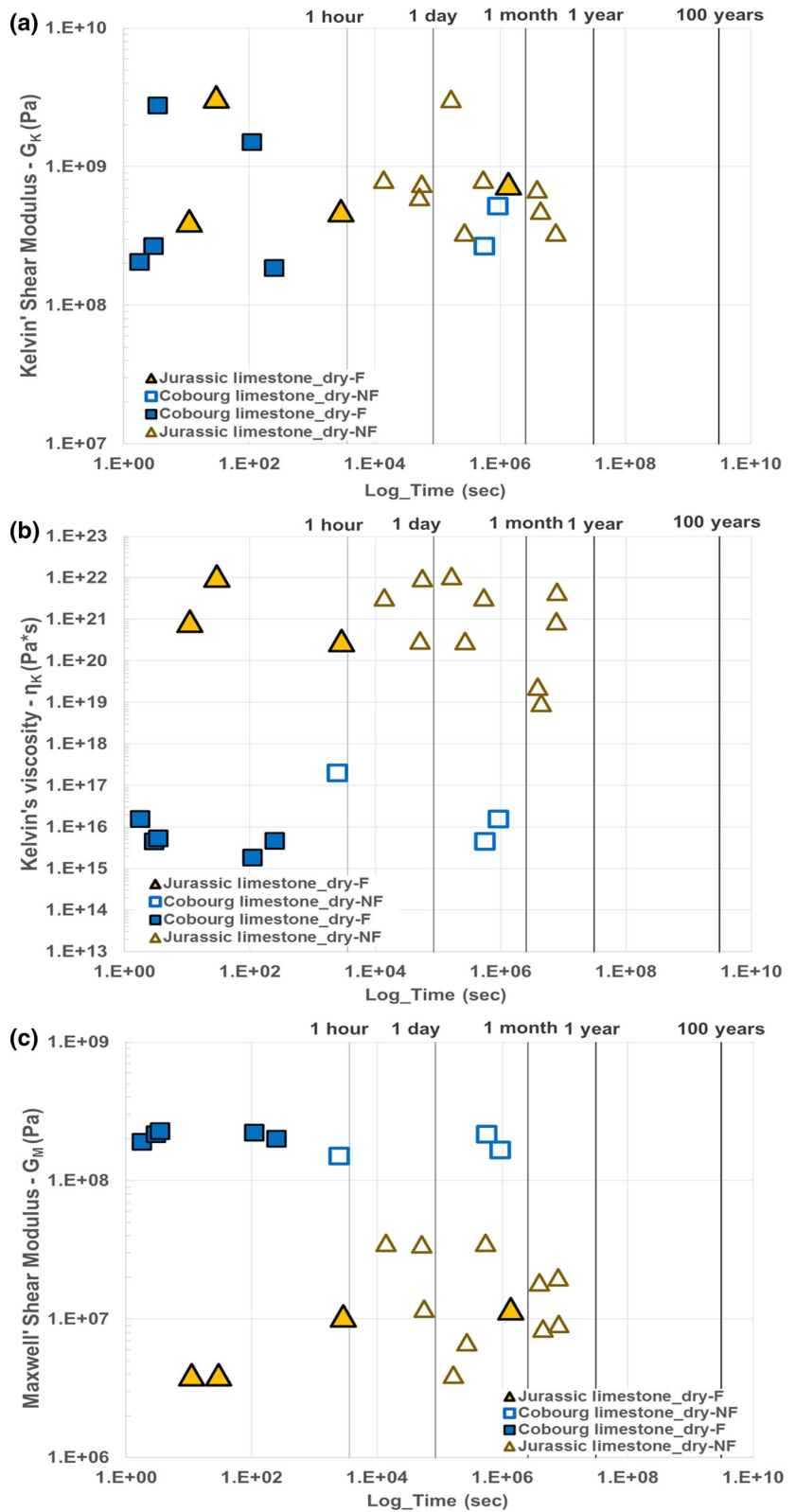


Fig. 22 Relating Time vs. Maxwell’s viscosity. The static load test data performed at room temperature in dry or wet conditions (stress levels can be referred to Fig. 15)

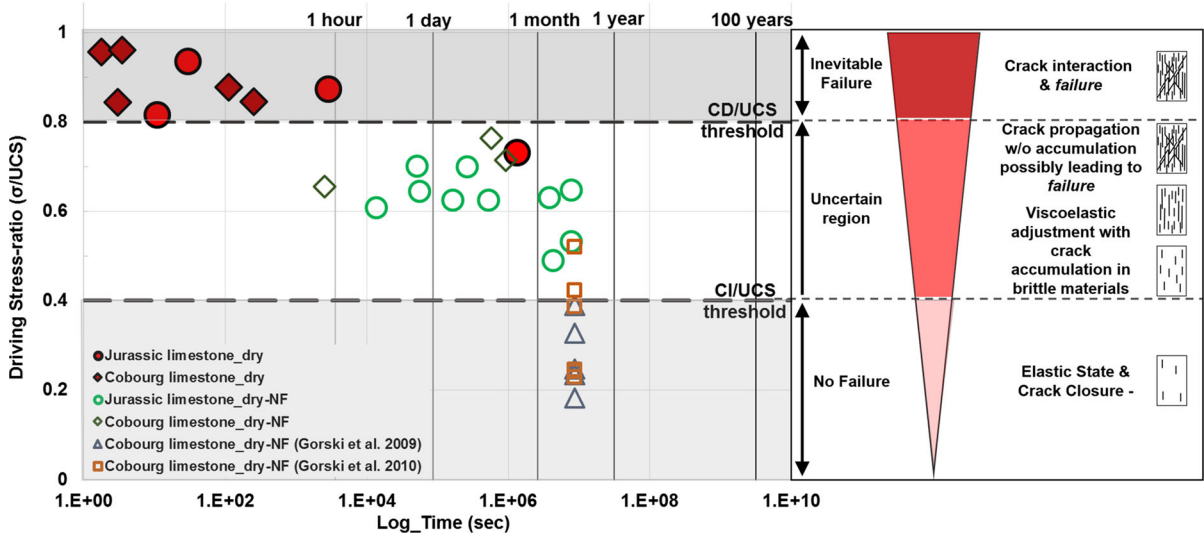
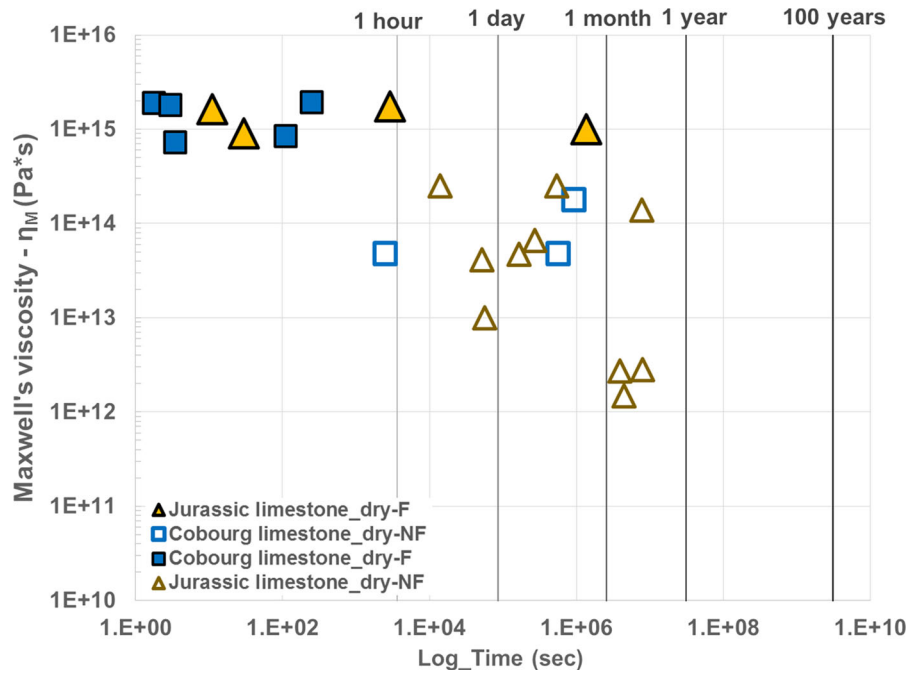


Fig. 23 Static load test data of Jurassic and Cobourg limestone performed at room temperature in dry conditions (where the driving stress-ratio is the stress level at failure to unconfined

compressive strength of the material). The ‘NF’ in the legend indicates that these samples or tests did not fail whereas the ‘F’ denotes that these samples or tests reach failure

stress-ratio to cause failure of the limestone would result in a longer time to failure than that derived for the granite. This is likely due to the grain scale heterogeneity in the granite (polymineralic components including quartz, feldspars and mica). These different minerals would have different creep rates. As

such there would be incompatible strains generated within the sample over time leading to internal stress concentrations and micro-cracking (damage and weakening). These processes are at work in the limestone as well but, given the more uniform mineralogy (more so in a pure limestone or marble)

the creep in the calcite minerals can occur with less associated damage and weakening (increased time to failure with more creep deformation).

Both the Jurassic and Cobourg limestone samples showed when the load was above the CD threshold, or 0.8 UCS, failure occurs within an hour. Below the CI threshold failure does not take place in the duration of the tested samples. When the applied axial stress ranges between the CD and CI thresholds, or 0.8 to 0.5 UCS, failure may occur during the first hours up to a month. In this driving stress range other parameters contributes to influence the long-term strength, such as the rate of flow or Maxwell's viscosity.

Not all tested samples reached failure in the present study. The 'non-failure' samples were studied in more detail to provide further insight into the long-term strength of brittle rocks. It was found that the more viscous samples were the ones that reached failure and that there was a clear division between failure and no failure at a Maxwell viscosities of $1E + 15$ (Pa s) and $1E + 14$ (Pa s), respectively.

The analysis presented herein described the procedure and examined the controlling factors during static

load testing, discussed the creep process, defined an analysis method, related the results to previous studies available in the literature and pointed to driving stress limit for failure and no failure with a region of uncertainty. Further research is required on the topic to investigate parameters that could better describe the time-dependent behaviour of rocks, enriching similar databases that engineers and practitioners could easily use as preliminary tools to both have an initial estimate of the materials' response and numerically simulate and back-analyze laboratory scale and in situ scale conditions where long-term deformations have a great impact on the rockmass behaviour.

Acknowledgements The authors would like to acknowledge funding for this research from the Nuclear Waste Organization of Canada (NWMO), The Natural Sciences and Engineering Research Council of Canada (NSERC) and the Scientific Equipment Program of ETH Zurich.

Appendix

See Tables 7, 8 and 9.

Table 7 Results from baseline testing for (a) Jurassic limestone and (b) Cobourg limestone

| Sample # | UCS (MPa) | CD (MPa) | CI (MPa) | E (GPa) | Poisson's ratio |
|--|-----------|----------|----------|---------|-----------------|
| <i>(a) Values for Jurassic limestone</i> | | | | | |
| 1 | 66 | 53 | 27 | 103 | 0.26 |
| 2 | 114 | 89 | 40 | 73 | 0.12 |
| 3 | 88 | 74 | 36 | 125 | 0.29 |
| 4 | 112 | 100 | 46 | 86 | 0.26 |
| 5 | 126 | 102 | 45 | 101 | 0.29 |
| 6 | 101 | 97 | 35 | 71 | 0.18 |
| 7 | 68 | 64 | 22 | 95 | 0.22 |
| 8 | 137 | 125 | 50 | 89 | 0.25 |
| 9 | 110 | 105 | 42 | 94 | 0.21 |
| 10 | 111 | 99 | 44 | 92 | 0.22 |
| <i>(b) Values for Cobourg limestone</i> | | | | | |
| 1 | 104 | 93 | 45 | 38 | 0.24 |
| 2 | 146 | 132 | 56 | 37 | 0.18 |
| 3 | 122 | 111 | 44 | 45 | 0.17 |
| 4 | 136 | 110 | 52 | 47 | 0.16 |
| 5 | 132 | 113 | 52 | 46 | 0.15 |
| 6 | 107 | 96 | 47 | 36 | 0.13 |
| 7 | 94 | 84 | 37 | 37 | 0.12 |
| 8 | 149 | 136 | 58 | 41 | 0.11 |
| 9 | 136 | 124 | 56 | 44 | 0.13 |

Table 8 Summary of elastic and mechanical properties estimating for (a) Jurassic limestone and (b) Cobourg limestone from the static load testing

| Sample name | CI (MPa) | E (GPa) | Poisson's ratio |
|--|----------|---------|-----------------|
| <i>(a) Values for Jurassic limestone</i> | | | |
| JURA_4S ^a | 52 | 41.3 | 0.12 |
| JURA_5S | 31 | 28.7 | 0.25 |
| JURA_6S | 50 | 31.3 | 0.14 |
| JURA_8S | 49 | 11.3 | 0.19 |
| JURA_9S ^a | 44 | 26.5 | 0.04 |
| JURA_37S | 46 | 32.8 | 0.13 |
| JURA_38S | 46 | 15.4 | 0.16 |
| JURA_42S | 52 | 31.2 | 0.16 |
| JURA_43S | 57 | 16.5 | 0.13 |
| JURA_44S | 24 | 8.1 | 0.13 |
| JURA_45S | 35 | 23.6 | 0.18 |
| JURA_46S | 35 | 23.6 | 0.18 |
| <i>(b) Values for Cobourg limestone</i> | | | |
| Cobourg_5S | 31 | 31.4 | 0.15 |
| Cobourg_7S | 41 | 43.2 | 0.25 |
| Cobourg_8S ^a | 40 | 30.3 | 0.13 |
| Cobourg_9S | 33 | 43.0 | 0.20 |
| Cobourg_12S | 31 | 52.9 | 0.28 |

^a Multi-step tests**Table 9** Summary of the static load testing results for (a) Jurassic limestone and (b) Cobourg limestone

| Sample name | Creep stress (MPa) | Time (s) | Driving stress-ratio (σ/UCS) | Crack Initiation stress-ratio (σ/CI) | Status (failure/no failure) |
|--|--------------------|-----------|---------------------------------------|---|-----------------------------|
| <i>(a) Values for Jurassic limestone</i> | | | | | |
| JURA_4S-1 ^a | 89 | 56,536 | 0.64 | 1.71 | NF |
| JURA_4S-2 ^a | 101 | 1,350,000 | 0.73 | 1.94 | F |
| JURA_5S | 72 | 2871 | 0.87 | 2.32 | F |
| JURA_6S | 93 | 52,294 | 0.70 | 1.86 | NF |
| JURA_8S | 91 | 269,817 | 0.70 | 1.86 | NF |
| JURA_9S-1 ^a | 71 | 13,937 | 0.61 | 1.61 | NF |
| JURA_9S-2 ^a | 73 | 537,297 | 0.62 | 1.66 | NF |
| JURA_37S | 79 | 7,861,686 | 0.65 | 1.72 | NF |
| JURA_38S | 65 | 7,868,315 | 0.53 | 1.41 | NF |
| JURA_42S | 87 | 3,888,000 | 0.63 | 1.67 | NF |
| JURA_43S | 74 | 4,417,200 | 0.49 | 1.30 | NF |
| JURA_44S | 52 | 11 | 0.81 | 2.17 | F |
| JURA_45S | 87 | 30 | 0.93 | 2.49 | F |
| JURA_46S | 58 | 166,537 | 0.62 | 1.66 | NF |
| <i>(b) Values for Cobourg limestone</i> | | | | | |
| Cobourg_5S | 66 | 251 | 0.84 | 2.13 | F |
| Cobourg_7S | 82 | 1.8 | 0.96 | 2.41 | F |

Table 9 continued

| Sample name | Creep stress (MPa) | Time (s) | Driving stress-ratio (σ/UCS) | Crack Initiation stress-ratio (σ/CI) | Status (failure/no failure) |
|---------------------------------|--------------------|----------|---------------------------------------|---|-----------------------------|
| <i>Cobourg_8S-1^a</i> | 66 | 2539 | 0.65 | 1.65 | NF |
| <i>Cobourg_8S-2^a</i> | 72 | 925,000 | 0.71 | 1.80 | NF |
| <i>Cobourg_8S-3^a</i> | 77 | 575,400 | 0.76 | 1.93 | NF |
| <i>Cobourg_8S-4^a</i> | 85 | 3 | 0.84 | 2.13 | F |
| <i>Cobourg_9S</i> | 73 | 112 | 0.88 | 2.21 | F |
| <i>Cobourg_12S</i> | 75 | 3.5 | 0.96 | 2.42 | F |

^a Multi-step tests

References

- Abass HH, Al-Mulhem AA, Alqam MS, Mirajuddin KR (2006) Acid fracturing or proppant fracturing in carbonate formation? A rock mechanic's view. In: Proceedings of SPE annual technical conference and exhibition held in San Antonio, Texas, USA
- Amitrano D, Helmstetter A (2006) Brittle creep, damage and time to failure in rocks. *J Geophys Res* 111(B11201):1–17
- Amitrano D, Grasso JR, Hantz D (1999) From diffuse to localized damage through elastic interaction. *Geophys Res Lett* 26(14):2109–2112
- Anagnostou G (2007) Practical consequences of the time-dependency of ground behaviour for tunnelling. In: Proceedings of rapid excavation and tunnelling conference, Toronto
- Anderson OL (1977) Stress-corrosion theory of crack propagation with applications to geophysics. *J Rev Geophys Space Phys* 15:77–104
- Apuani T, Masetti M, Rossi M (2007) Stress–strain–time numerical modelling of a deep-seated gravitational slope deformation: preliminary results. *Quatern Int* 171–172:80–89
- ASTM (2008) Standard test methods for creep of rock core under constant stress and temperature, D7070-08
- Aydan O, Akagi T, Kawamoto T (1993) The squeezing potential of rocks around tunnels; theory and prediction. *J Rock Mech Rock Eng* 26(2):137–163
- Aydan O, Akagi T, Kawamoto T (1996) The squeezing potential of rock around tunnels: theory and prediction with examples taken from Japan. *J Rock Mech Rock Eng* 29(3):125–143
- Barla G, Bonini M, Debernardi D (2008) Time dependent deformations in squeezing tunnels. In: Proceedings of the 12th international conference of international association for computer methods and advances in geomechanics (IACMAG), Goa, India
- Barla G, Bonini M, Debernardi D (2010) Time dependent deformations in squeezing tunnels. *Int J Geoenviron Eng* 2(1):819–824
- Barton NR (1974) Estimating the shear strength of rock joints. In: Proceedings of the 3rd congress, ISRM. Denver, pp 1–7
- Berest P, Blum P, Charpentier J, Gharbi H, Vales F (2005) Very slow creep tests on rock samples. *Int J Rock Mech Min Sci* 42:569–576
- Besterfield DH (1979) Quality control. Prentice-Hall, Englewood Cliffs, p 309
- Bieniawski T (1967) Mechanism of brittle fracture of rock, parts I, II, and III. *Int J Rock Mech Min Sci* 4(4):395–430
- Bieniawski T (1974) Geomechanics classification of rock-masses and its application in tunnelling. In: Proceedings of the 3rd congress, ISRM, Denver
- Bonini M, Debernardi D, Barla M, Barla G (2009) The mechanical behaviour of clay shales and implications on the design of tunnels. *J Rock Mech Rock Eng* 42(2):361–388
- Boukharov GN, Chanda MW, Boukharov NG (1995) The three processes of brittle crystalline rock creep. *Int J Rock Mech Min Sci Geomech* 32(4):325–335
- Brace WR, Paulding BW Jr, Scholz C (1966) Dilatancy in the fracture of crystalline rocks. *J Geophys Res* 71(3939–3953):40–65
- Brantut N, Heap MJ, Meredith PG, Baud P (2013) Time-dependent cracking and brittle creep in crustal rocks: a review. *J Struct Geol* 52:17–43
- Charles R (1959) The static fatigue of glass. *J Appl Phys* 29:1549–1560
- Chen G, Chugh Y (1996) Estimation of in situ visco-elastic parameter of weak floor strata by plate-loading tests. *J Geotech Geol Eng* 14(2):151–167
- Chin HP, Rogers DJ (1987) Creep parameters of rocks on an engineering scale. *Rock Mech Rock Eng* 20:137–146
- Chugh YP, Nath R, Shankar S (1987) Time-dependent behaviour of immediate weak floor strata from an Illinois coal mine. In: Proceedings of 6th international conference on ground control in mining, West Virginia University, Morgantown, WV, pp 204–218
- Colback PSB, Widd BL (1965) The influence of moisture content of compressive strength of rock. In: Proceedings of 3rd Canadian rock mechanics symposium, Toronto, pp 65–83
- Cristescu ND (2009) Time effects in rock mechanics. In: Proceedings of the SME annual conference, Albuquerque, New Mexico
- Cruden DM (1974) The static fatigue of brittle rock under uniaxial compression. *Int J. Rock Mech. Mine Sci* 11:67–73
- da Andrade ENC (1910) On the viscous flow in metals and allied phenomena. *Proc R Soc Lond A* 84:1–12
- Danjanac B, Fairhurst C (2010) Evidence for a long-term strength threshold in crystalline rock. *J Rock Mech Rock Eng* 43(5):513–531

- Davis GH, Reynolds SJ, Kluth CF (2012) Structural geology of rocks and regions, 3rd edn. Wiley, New York. ISBN 978-1-118-21505-0
- Debernardi D (2008) Viscoplastic behaviour and design of tunnels. Ph.D. thesis. Politecnico di Torino, Italy
- Diederichs MS (1999) Instability of hard rockmasses: the role of tensile damage and relaxation. Ph.D. thesis, University of Waterloo, Waterloo, ON, Canada
- Diederichs MS (2003) Rock fracture and collapse under low confinement conditions. *J Rock Mech Rock Eng* 36(5):339–381
- Diederichs MS, Martin CD (2010) Measurement of spalling parameters from laboratory testing. In: Proceedings of Eurock, Lausanne, Switzerland
- Diederichs MS, Kaiser PK, Eberhardt E (2004) Damage initiation and propagation in hard rock during tunnelling and the influence of near-face stress rotation. *Int J Rock Mech Min Sci* 41(5):785–812
- Dragon A, Mroz Z (1979) A model for plastic creep of rock-like materials accounting for the kinetics of fracture. *Int J Rock Mech Min Sci Geomech* 16:253–259
- Dunham RJ (1962) Classification of carbo-hidenate rocks according to depositional texture. In: HamWE (ed) Classification of carbo-hidenate rocks: American association of petroleum geologists memoir, pp 108–121
- Dusseault MB, Fordham CJ (1993) Time-dependent behaviour of rocks. In: Hudson JA (ed) Comprehensive rock engineering, vol 3. Pergamon Press, Oxford, pp 119–149
- Eberhardt E, Stead D, Stimpson B, Read RS (1998) Identifying crack initiation and propagation thresholds in brittle rock. *Can Geotech J* 35:222–233
- Einstein HH (1996) Tunnelling in difficult ground—swelling behaviour and identification of swelling rocks. *J Rock Mech Rock Eng* 29(3):113–124
- Fairhurst C, Cook NGW (1966) The phenomenon of rock splitting parallel to the direction of maximum compression in the neighborhood of a surface. In: Proceedings of the 1st congress on the international society of rock mechanics, National Laboratory of Civil Engineering, Lisbon, Portugal, vol 1, pp 687–692
- Feng XT, Chen BR, Yang CX, Zhiou H (2006) Intelligent analysis of rheological characteristic of rock materials. In: Proceedings of multiphysics coupling and long-term behaviour of rock mechanics, pp 275–280
- Fifer Bizjak K, Zupancic A (2009) Site and laboratory investigation of the Slano blato landslide. *Eng Geol* 105:171–185
- Ghazvnian E (2015) Fracture initiation and propagation in low porosity crystalline rocks: implications for excavation damage zone (EDZ) mechanics. Ph.D. thesis, Queen's University, Canada
- Gioda G (1981) A finite element solution of non-linear creep problems in rocks. *J Rock Mech Sci Geomech* 18:35–46
- Glamheden R, Hokmark H (2010) Creep in jointed rockmasses. State of the knowledge. SKB
- Goodman R (1980) Introduction to rock mechanics, 1st edn. Wiley, New York
- Gorski B, Anderson T, Conlon B (2009) DGR site characterization documents, technical reports TR-08-11. www.nwmo.ca
- Gorski B, Anderson T, Conlon B (2010) DGR site characterization documents, technical reports TR-08-36. www.nwmo.ca
- Gruden DN (1971) Single-increment creep experiments on rock under uniaxial compression. *Int J Rock Mech Min Sci* 8:127–142
- Guan Z, Jiang Y, Tanabashi Y, Huang H (2008) A new rheological model and its application in mountain tunnelling. *J Tunnel Under Space Tech* 23:292–299
- Hagros A, Johanson E, Hudson JA (2008) Time dependency in the mechanical properties of crystalline rocks: a literature survey. Possiva OY, Finland
- Hao SW, Zhang BJ, Tian JF, Elsworth D (2014) Predicting time-to-failure in rock extrapolated from secondary creep. *J Geophys Res Solid Earth* 119:1942–1953
- Hardy HR Jr, Kim RY, Stefanko R, Wang YJ (1970) Creep and microseismic activity in geologic materials. In: Proceedings of 1st symposium on rock mechanics (AIME), pp 377–414
- Harvey DR (1967) Thermal expansion of certain Illinois limestones and dolomites. State of Illinois Department of Registration and Education, Illinois State Geological Survey, Urbana, Illinois
- Heap MJ, Baud P, Meredith PG, Vinciguerra S, Bell AF, Main IG (2011) Brittle creep in basalt and its application to time-dependent volcano deformation. *J Earth Planet Sci Lett* 37(1–2):71–82
- Hoek E, Brown T (1980) Underground excavations in rock. Institution of Mining and Metallurgy, London
- Hudson JA, Harrison JP (1997) Engineering rock mechanics—an introduction to the principles. Elsevier, Oxford
- ISRM (1979) Suggested methods for determining the uniaxial compressive strength and deformability of rock materials. 16(2):138–140
- ISRM (2014) Suggested methods for determining the creep characteristics of rock. 47:275–290
- Jandakaew M (2007) Stress-path dependency of rock salt, rock mechanics, Fuenkajorn & Phien-wej (eds), pp 171–188
- Kawada Y, Nagahama H (2004) Viscoelastic behaviour and temporal fractal properties of Iherzolite and marble. *Terra Nova* 16:128–132
- Korzeniowski W (1991) Rheological model of hard rock pillar. *J Rock Mech Rock Eng* 24:155–166
- Kranz RL, Scholz CH (1977) Critical dilatant volume of rocks at the onset of tertiary creep. *J Geophys Res* 82(4):893–894, 898
- Kranz R, Harris WJ, Carter NL (1982) Static fatigue of granite at 200 C. *J Geophys Res* 9:1–4
- Ladanyi B, Gill DE (1988) Design of tunnel linings in a creeping rock. *Int J Min Geol Eng* 6:113–126
- Lajtai EZ (1974) Brittle failure in compression. *Int J Fract* 10(4):525–536
- Lajtai EZ (1998) Microscopic fracture processes in a granite. *J Rock Mech Rock Eng* 31:237–250
- Lajtai E, Bielus LP (1986) Stress corrosion cracking of Lac du Bonnet granite in tension and compression. *Rock Mech Rock Eng* 19:71–87
- Lajtai EZ, Schmidtke RH (1986) Delayed failure in rock loaded in uniaxial compression. *Rock Mech Rock Eng* 19:11–25
- Lajtai EZ, Duncan J, Carter J (1991) The effect of strain rate on rock strength. *J Rock Mech Rock Eng* 24:99–109
- Lau JSO, Conlon B (1997) Long-term loading tests on Lac du Bonnet pink granite. Report MMSL 97-076(CR), CANMET, Natural Resources Canada

- Lau J, Gorski B, Conlon B, Anderson T (2000) Long-term loading tests on saturated granite and granodiorite, CANMET
- Lauffer H (1958) Gebirgsklassiferung fuer den Stollenbau. *Geol Bauwes* 24:46–51
- Lin Q (2006) Strength degradation and damage micromechanism of granite under long-term loading. Ph.D., University of Hong-Kong
- Liu X, Yang X, Wang J (2016) A nonlinear creep model of rock salt and its numerical implement in FLAC3D. *Adv Materi Sci Eng* 285158. doi:10.1155/2015/285158
- Lockner D (1993) Room temperature creep in saturated granite. *J. Geophys Res* 98:475–487
- Lockner DJ, Byrlee (1980) Development of fracture planes during creep in granite. In: Proceedings of 2nd conference on acoustic emission/microseismic activity in geological structures and materials. Trans Tech Publication, Claus-thal-Zellerfeld, pp 11–25
- Lockner DA, Moore DE, Reches Z (1992) Microcrack intersection leading to fracture. *Rock mechanics*. Balkema, Rotterdam, pp 807–816
- Malan DF, Vogler UW, Drescher K (1997) Time-dependent behaviour of hard rock in deep level gold mines. *J South Afr Inst Min Metall* 97:135–147
- Marcato G, Mantovani M, Pasuto A, Tagliavini F, Silvano S, Zabuski L (2009) Assessing the possible future development of the Tessina landslide using numerical modelling, mountain risks. In: Proceeding of the 6th framework program of the European Commission. Italy
- Martin CD (1993) The strength of massive Lac du Bonnet granite around underground openings. Ph.D. thesis, University of Manitoba
- Martin CD (1997) Seventeenth Canadian geotechnical colloquium: the effect of cohesion loss and stress path on brittle rock strength. *Can Geotech J* 34(5):698–725
- Martin D, Chandler A (1994) The progressive fracture of Lac du Bonnet granite. *J Rock Mech Min Sci Geomech* 31(6):643–659
- Martin CD, Kaiser PK, McCreath DR (1999) Hoek–Brown parameters for predicting the depth of brittle failure around tunnels. *Can Geotech J* 36(1):136–151
- Minkley W, Menzel W, Konietzky H, te Kamp L (2001) A visco-elasto-plastic softening model and its application for solving static and dynamic stability problems in potash mining. In: Proceedings of 2nd international FLAC symposium, Lyon
- Nicksiar M, Martin CD (2012) Evaluation of methods for determining crack initiation in compression tests on low-porosity rocks. *J Rock Mech Rock Eng* 45(4):607–617
- Ottosen NS (1986) Visco-elastic-viscoplastic formulas for analysis in rock salt cavities. *Int J Rock Mech Min Struct Geomech Abstr* 23(3):201–212
- Palmstrom A (1995) RMI—a rockmass characterization system for rock engineering purposes. Ph.D. thesis. University of Oslo, Norway, p 400
- Paraskevopoulou C (2016) Time-dependency of rocks and implications associated with tunnelling. Ph.D. thesis
- Paraskevopoulou C, Benardos A (2013) Assessing the construction cost of tunnel projects. *Tunn Undergr Space Technol* 38:497–505
- Paraskevopoulou C, Perras M, Diederichs MS, Amaan F, Löw S, Lam T (2015) Long-term static load laboratory testing behaviour of different rock types. In: Proceedings of the Canadian geotechnical symposium GeoQuebec on challenges from North to South. Quebec
- Paraskevopoulou C, Perras M, Diederichs MS, Löw S (2017) The three stages of stress-relaxation - observations for the long-term behaviour of rocks based on laboratory testing. *J Eng Geol* 216:56–75
- Pellet FL (2010) Large time-dependent convergences in a tunnel excavated in a carboniferous rockmass. In: Proceeding of the 6th Asian rock mechanics symposium, New Delhi, India, No 79
- Pellet F, Hajdu A, Deleruyelle F, Bensus F (2005) A viscoplastic model including anisotropic damage for the time-dependent behaviour of rock. *Int J Numer Anal Methods Geomech* 29:941–970
- Peng SS (1973) Relaxation and the behaviour of failed rock. *Int J Rock Mech Min Sci Geomech* 10:235–246
- Perras MA, Diederichs MS (2014) A review of the tensile strength of rock: concepts and testing. *J Geotech Geol Eng* 32:525–546
- Perras MA, Diederichs MS (2016) Predicting excavation damage zone depth in brittle rock. *J Rock Mech Geotech Eng* 8(1):60–74
- Perzyna P (1966) Fundamental problems in viscoplasticity. *Adv Appl Mech* 9(2):244–368
- Pimienta L, Fortin J, Gueguen Y (2014) Investigation of elastic weakening in limestone and sandstone samples from moisture adsorption. *Int J Geophys* 199:335–347
- Podnieks ER, Chamberlain PG, Thill RE (1968) Environmental effects on rock properties. In: Proceedings of the tenth symposium of rock mechanics, University of Missouri at Rolla
- Potyondy D (2007) Simulating stress corrosion with a bonded-particle model for rock. *Int J Rock Mech Min Sci* 44:677–693
- Rahman SS, Kagan M, Marx C (1992) Prediction of borehole stability in tar sands with the use of a rheological model. *J Energy Sources* 14:225–240
- Schmidtke H, Lajtai Z (1985) The long-term strength of Lac du Bonnet granite. *J Rock Mech Min Sci Geotech* 22:461–465
- Scholz CH (1968) Mechanism of creep in brittle rock. *J Geophys Res* 73(10):3295–3302
- Sharifzadeh M, Tarifard A, Moridi MA (2013) Time-dependent behaviour of tunnel lining in weak rockmass based on displacement back analysis method. *J Tunn Undergr Space Technol* 38:348–356
- Singh DP (1975) A study of creep of rocks. *Int J Rock Mech Sci Geomech* 12:271–276
- Singh AK, Balasingh C, Mao H-K, Hemley RJ, Shu J (1998) Analysis of lattice strains measured under nonhydrostatic pressure. *J Appl Phys* 83:7567–7575
- Sofianos A, Nomikos P (2008) Advanced rock mechanics, course notes, N.T.U.A
- Stagg KG, Zienkiewicz OC (1986) *Rock mechanics in engineering practice*. Wiley, New York
- Sterpi D, Gioda G (2009) Visco-plastic behaviour around advancing tunnels in squeezing rock. *J Rock Mech Rock Eng* 42:319–339

- Van P, Szarka Z (2006) Rock rheology—time dependence of dilation and stress around a tunnel. In: Proceedings of the international symposium of the international society for rock mechanics, Eurock 2006, Belgium
- Wawesik WR (1972) Time-dependent rock behaviour in uniaxial compression. In: Proceedings of 14th rock mechanics symposium, University of Pennsylvania, pp 85–106
- Weaver SH (1936) Creep curve of steel. *Trans Am Soc Mech Eng*, LVIII, pp 745–751
- Widd BL (1966) The time-dependent behaviour of rock; Considerations with regard to a research program. CSIR report MEG 514, Rock Mechanics Division, National Mechanical Engineering Research Institute, Pretoria, South Africa
- Widd BL (1970) The influence of moisture on the pre-rupture fracturing of two rock types. In: Proceedings 2nd congress international society for rock mechanics, Belgrade, vol 2, pp 239–245
- Zhang H, Wang Z, Zheng Y, Duan P, Ding S (2012) Study on tri-axial creep experiment and constitutive relation of different rock salt. *Saf Sci* 50(4):801–815.
- Zhifa Y, Zhiyin W, Luqing Z, Ruiguang Z, Nianxing X (2001) Back-analysis of visco-elastic displacements in a soft rock road tunnel. *Int J of Rock Mech Min Sci* 38:331–341